

# Identification and characterization of science-rich landing sites for lunar lander missions using integrated remote sensing observations

J. Flahaut<sup>a,\*</sup>, J.-F. Blanchette-Guertin<sup>b</sup>, C. Jilly<sup>c</sup>, P. Sharma<sup>d</sup>, A. Souchon<sup>e,f</sup>,  
W. van Westrenen<sup>g</sup>, D.A. Kring<sup>h</sup>

<sup>a</sup> Laboratoire de Géologie de Lyon, UMR 5276 du CNRS, ENS Lyon/Université Lyon 1, 2 rue Raphaël Dubois, 69622 Villeurbanne Cedex, France

<sup>b</sup> Department of Earth and Ocean Sciences, University of British Columbia, 6339 Stores Road, Vancouver, BC, Canada, V6E 3M2

<sup>c</sup> Hawai'i Institute of Geophysics and Planetology, University of Hawai'i at Manoa, Honolulu, Hawaii 96822, USA

<sup>d</sup> Lunar and Planetary Laboratory, University of Arizona, 1629 E. University Blvd, Tucson, AZ 85721, USA

<sup>e</sup> Université de Toulouse III, Observatoire Midi-Pyrénées, UPS-OMP, IRAP, Toulouse, France

<sup>f</sup> CNRS, UMR 5277, IRAP, 14, Avenue Edouard Belin, F-31400 Toulouse, France

<sup>g</sup> Faculty of Earth and Life Sciences, VU University Amsterdam, De Boelelaan 1085, 1081 HV Amsterdam, The Netherlands

<sup>h</sup> Lunar and Planetary Institute, USRA, 3600 Bay Area Blvd., Houston, TX 77058, USA

Available online 30 May 2012

## Abstract

Despite more than 52 years of lunar exploration, a wide range of first-order scientific questions remain about the Moon's formation, temporal evolution, and current surface and interior properties. Addressing many of these questions requires obtaining new *in situ* analyses or return of lunar surface or shallow subsurface samples, and hence rely on the selection of optimal landing sites. Here, we present an approach to optimize science-rich lunar landing site selection studies based on the integration of remote sensing observations. Currently available remote sensing data, as well as features of interest published in the recent literature, were integrated in a Geographic Information System. This numerical database contains geographic information about all these findings, which can be consulted and used to simultaneously display multiple features and parameters of interest. To illustrate our approach, we identified the optimal landing sites to address the two top priorities (or goals) relative to Concept 3 of the National Research Council of the National Academies (2007), namely to 'Determine the extent and composition of the primary feldspathic crust, (ur)KREEP layer, and other products of differentiation' and to 'Inventory the variety, age, distribution and origin of lunar rock types'. We review site requirements and propose possible landing sites for both these goals. We identified 29 sites that best fulfill both these goals and compare them with the landing sites of planned future lunar lander missions. Finally, we detail two of these science-rich sites (Aristarchus and Theophilus craters) which are particularly accessible through their location on the nearside.

© 2012 COSPAR. Published by Elsevier Ltd. All rights reserved.

**Keywords:** Moon; Landing sites; Exploration; Remote sensing; Database; Crustal diversity

## 1. Introduction

In the wake of the publication of the NASA Vision for Space Exploration (January, 2004), major publications by

Jolliff et al. (2006) and the US National Research Council of the National Academies (NRC, 2007) highlighted the main remaining scientific challenges and opportunities for future lunar exploration missions. The NRC report provided a clear overview of priorities and recommendations for scientific lunar exploration, summarized in Table 1. Many of the scientific priorities listed in Table 1 require performing *in situ* analyses of lunar surface or shallow subsurface samples, and hence rely on the selection of optimal landing sites. Successful missions by the USA (Clementine,

\* Corresponding author. Tel.: +33 6 18 48 36 12; fax: +33 4 72 44 85 93.

E-mail addresses: [jessica.flahaut@ens-lyon.org](mailto:jessica.flahaut@ens-lyon.org) (J. Flahaut), [jguertin@eos.ubc.ca](mailto:jguertin@eos.ubc.ca) (J.-F. Blanchette-Guertin), [cjilly@hawaii.edu](mailto:cjilly@hawaii.edu) (C. Jilly), [psharma@lpl.arizona.edu](mailto:psharma@lpl.arizona.edu) (P. Sharma), [souchon@ntp.obs-mip.fr](mailto:souchon@ntp.obs-mip.fr) (A. Souchon), [wim.van.westrenen@falw.vu.nl](mailto:wim.van.westrenen@falw.vu.nl) (W. van Westrenen), [kring@lpi.usra.edu](mailto:kring@lpi.usra.edu) (D.A. Kring).

Table 1  
List of the top 11 lunar science priorities (NRC, 2007).

Priority	Goal	Title
1	1a	Test the cataclysm hypothesis by determining the spacing in time of the creation of the lunar basins
2	1b	Anchor the early Earth–Moon impact flux curve by determining the age of the oldest lunar basin (South Pole-Aitken Basin)
3	1c	Establish a precise absolute chronology
4	4a	Determine the compositional state (elemental, isotopic, mineralogical) and compositional distribution (lateral and depth) of the volatile component in lunar polar regions
5	3A	Determine the extent and composition of the primary feldspathic crust, KREEP layer, and other products of planetary differentiation
6	2a	Determine the thickness of the lunar crust (upper and lower) and characterize its lateral variability on regional and global scales
7	2b	Characterize the chemical/physical stratification in the mantle, particularly the nature of the putative 500-km discontinuity and the composition of the lower mantle
8	8a	Determine the global density, composition, and time variability of the fragile lunar atmosphere before it is perturbed by further human activity
9	2c	Determine the size, composition, and state (solid/liquid) of the core of the Moon
10	3B	Inventory the variety, age, distribution, and origin of lunar rock types
11	8b	Determine the size, charge, and spatial distribution of electrostatically transported dust grains and assess their likely effects on lunar exploration and lunar-based astronomy

Lunar Prospector, Lunar Reconnaissance Orbiter LRO/LCROSS), Europe (SMART-1), China (Change'E-1 and Chang'E-2), Japan (SELENE), and India (Chandrayaan-1), and state-of-the-art analyses of Apollo-era samples and data are rapidly expanding the database that can be used for landing site selection studies. In the coming years, the quantity and quality of lunar remote sensing data is expected to increase even further through institutional agency science missions such as LADEE, GRAIL, Luna-Glob 1, and Chandrayaan-2. In addition, several agencies are developing lunar lander missions (e.g., ESA Lunar Lander, Chang'E-3 and -4, Luna-Glob 2, Luna-Grunt, SELENE-2), and there is the distinct possibility of non-agency missions to the lunar surface carrying small scientific payloads, for example through teams vying to win the Google Lunar X-Prize (GLXP) (<http://www.googlelunarxprize.org>).

The widening range and improving quality of recent and upcoming remote sensing data form an ideal basis for performing landing site selection studies. Here, we show how

the integration of a large range of available datasets (obtained at different spatial resolutions from different missions) can be employed to identify lunar landing sites with maximum scientific potential. We gathered, processed, and geo-referenced many available datasets from previous lunar orbital missions into a Geographic Information System (GIS) which provides mapping and calculation tools. We also included information from sections of as yet unreleased datasets that were published in recent literature, as well as estimates of the depth of origin of material found in impact craters. The GIS provides a complete numerical database of older and recent lunar findings, which can be consulted and used to display features and parameters of interest.

In principle, our methodology can be applied to the selection of optimal landing sites for lunar landing missions of any type and size (i.e. lander only, lander plus rover, manned landings), and for addressing any of the prioritized NRC report goals listed in Table 1. We illustrate our

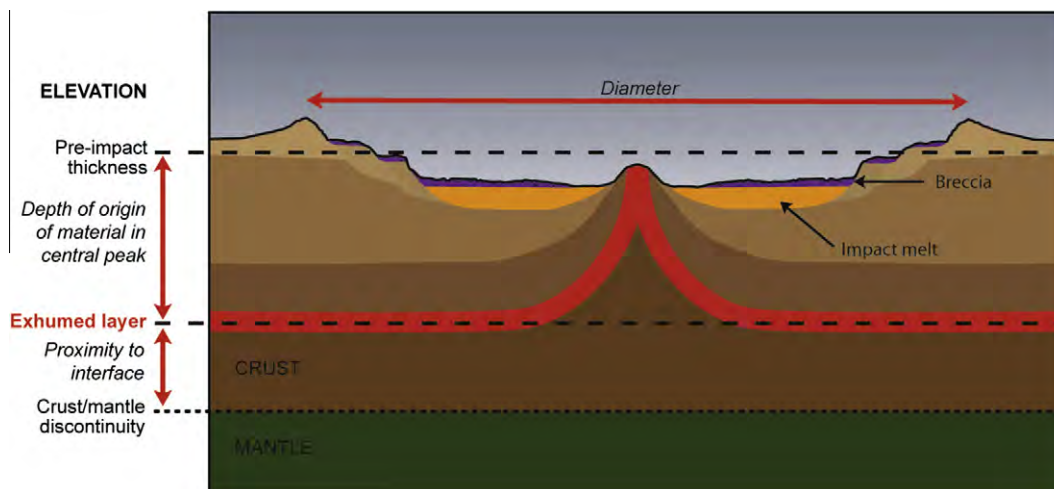


Fig. 1. Schematic cross section of a complex impact crater exhuming deep layers in its central peak. For each of these craters the proximity to the lunar crust-mantle boundary was calculated by subtracting the depth of origin ( $D_e$  or  $D_m$ , excavation depth and melting depth, respectively) from the crustal thickness ( $T$ ). Here proximity to the crust-mantle boundary ( $P_m$ , melt proximity) via the maximum depth of origin is illustrated.

Table 2

List of all the available global maps used to define regions of interest, with their mission of origin, digital resolution, and source. Abbreviations: USGS = United States Geological Survey ([www.usgs.gov](http://www.usgs.gov)), PDS = Planetary Data System (NASA, [pds.nasa.gov](http://pds.nasa.gov)), LPI = Lunar and Planetary Institute (USRA, [www.lpi.usra.edu](http://www.lpi.usra.edu)).

Data	Mission	Spatial resolution	Source
Clementine UVVIS global map (5 bands) and derived products (RBG)	Clementine	200 m/px	USGS
Clementine UVVIS 750 nm filter albedo map	Clementine	100 m/px	USGS
Lunar Orbiter global mosaic	Lunar Orbiter	60 m/px	USGS
FeO global distribution map	Clementine	100 m/px	USGS, Lucey et al. (1998)
	Lunar Prospector	15 km/px	PDS
TiO global distribution map	Clementine	100 m/px	USGS, Lucey et al. (2000)
	Lunar Prospector	60 km/px	PDS
Th and H global distribution maps	Lunar Prospector	15 km/px	PDS
K and Sm global distribution maps	Lunar Prospector	60 km/px	PDS
Al, Ca, Mg, Si, O global distribution maps	Lunar Prospector	150 km/px	PDS
Lunar Impact Crater Database			LPI
Crustal thickness maps	Clementine	30 km/px	Wieczorek and Phillips (1998)
topographic maps	Clementine	1.9 km/px	USGS
	LRO (LOLA)	470 m/px	PDS

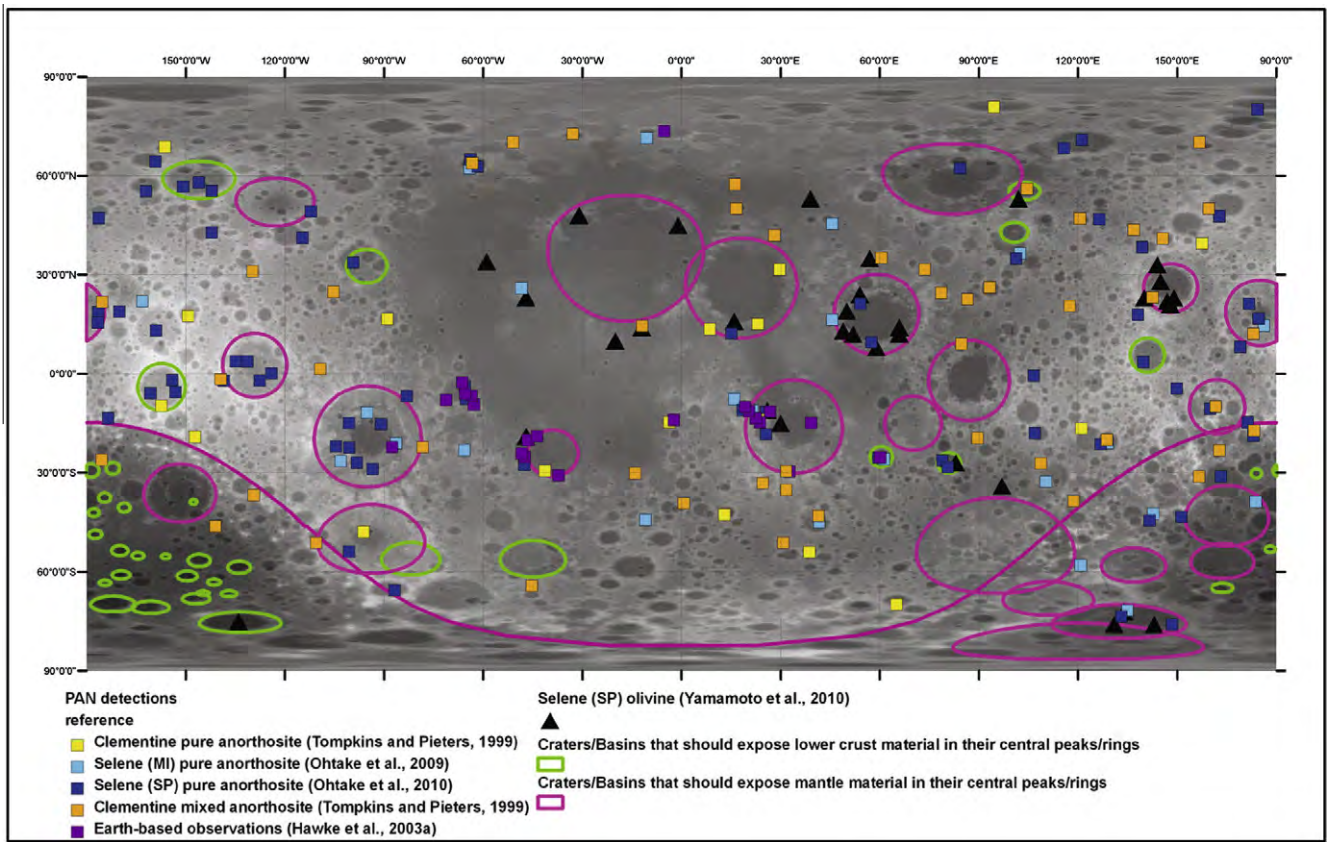


Fig. 2. Map of suggested sites to sample the primary products of lunar differentiation. Purest anorthosite (PAN) detections from different missions and sources (Tompkins and Pieters, 1999; Hawke et al., 2003a,b; Ohtake et al., 2009, 2010; cf. Appendix B) are represented by squares. Circular features represent all the craters or basins that should have exhumed lower crust (in green) and/or mantle (in purple) material in their central peaks or uplifted rings. The complete list of craters mapped is provided in Appendix A.

approach with case studies focusing on landing sites that can best deliver the prioritized goals related specifically to Concept 3 of the NRC report: (3A) ‘Determine the extent and composition of the primary feldspathic crust, KREEP layer and other products of differentiation’ and (3B) ‘Inventory the variety, age, distribution and origin of lunar

rock types’. Concept 3 was chosen for this article based on previous work done by the team of authors (Flahaut et al., 2011; Blanchette-Guertin et al., 2011; Jilly et al., 2011; Sharma et al., 2011; Souchon et al., 2011; LEIP, 2010). We demonstrate the results of our investigation by focusing on two landing sites of particular importance for crustal

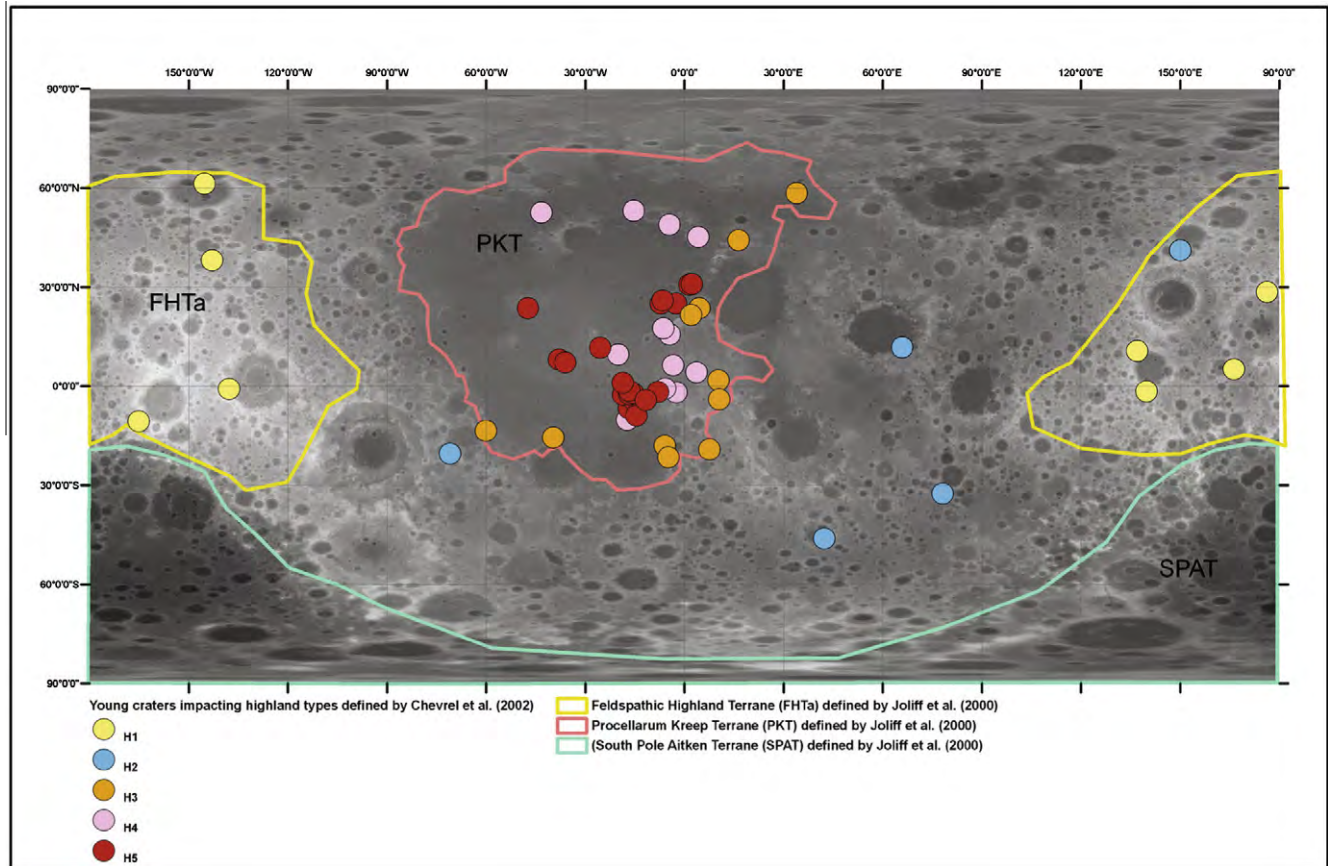


Fig. 3. Combined map showing the outline of the 3 main geochemical terranes defined by Jolliff et al. (2000), with the distribution of fresh craters (Copernican or rayed) that are impacting one of the five highland types defined by Chevrel et al. (2002) (List in Appendix C). Sampling H1 and H2 highland types, which are more likely to represent remains of the lunar magma ocean, is a priority for requirements A1 and A2. Any place located within the 3 distinct terranes is a possible landing site to fulfill requirement A3, but samples for the 3 terranes are required, implying multiple landings.

rock diversity studies, and provide a detailed characterization of these sites.

## 2. Datasets and methods

### 2.1. GIS setup

We used the ArcGIS software from ESRI to build a GIS to integrate data from different lunar missions. A list of all the publicly released datasets that were used for this study is presented in Table 2. Clementine and Lunar Orbiter global maps were used as a background for more recent Lunar Reconnaissance Orbiter Camera (LROC) images (Robinson et al., 2010). A Lunar Orbiter Laser Altimeter (LOLA) Digital Elevation Model (DEM) at 64 pixels per degree (approximately 470 meters per pixel) was added to this image collection, providing elevation data (Smith et al., 2010). The LOLA data were used to create topographic profiles of regions of interest and to create slope map to help identify scarps. The base map in Figs. 2–7 of this paper is the grayscale version of the LOLA topography.

The composition of the lunar surface was studied with both Clementine RGB and Lunar Prospector global maps. Clementine RGB images are made using ratios of UVVIS

bands from the multispectral imager (as described in Heather and Dunkin, 2002). The color ratio image product serves to cancel out the dominant surface brightness variations (controlled by albedo variations and topographic shading) and enhances color differences related to soil mineralogy and maturity. The lunar highlands, mostly old (>4 Ga) gabbroic anorthosite rocks, are dominated by shades of red (old) and blue (younger). The lunar maria (~3.9 to ~1 Ga based on crater density distributions, e.g., Hiesinger et al., 2003), mostly iron-rich basaltic materials of variable titanium content, are portrayed in shades of yellow/orange (iron-rich, lower titanium) and blue (iron-rich, higher titanium). Superimposed on and intermingled with these basic units are materials from basins and craters of various ages, ranging from the dark reds and blues of ancient basins to the bright blue crater rays of younger craters (e.g., McEwen et al., 1994; Pieters et al., 1994). Although the relatively low resolution of this map is not optimal for local-scale surveys, it provides an informative first order assessment of the variety of rocks in a certain area.

Contour maps were also generated using both Lunar Prospector (Lawrence et al., 1998, 2002) and Clementine elemental abundance (Lucey et al., 1998, 2000) maps, to

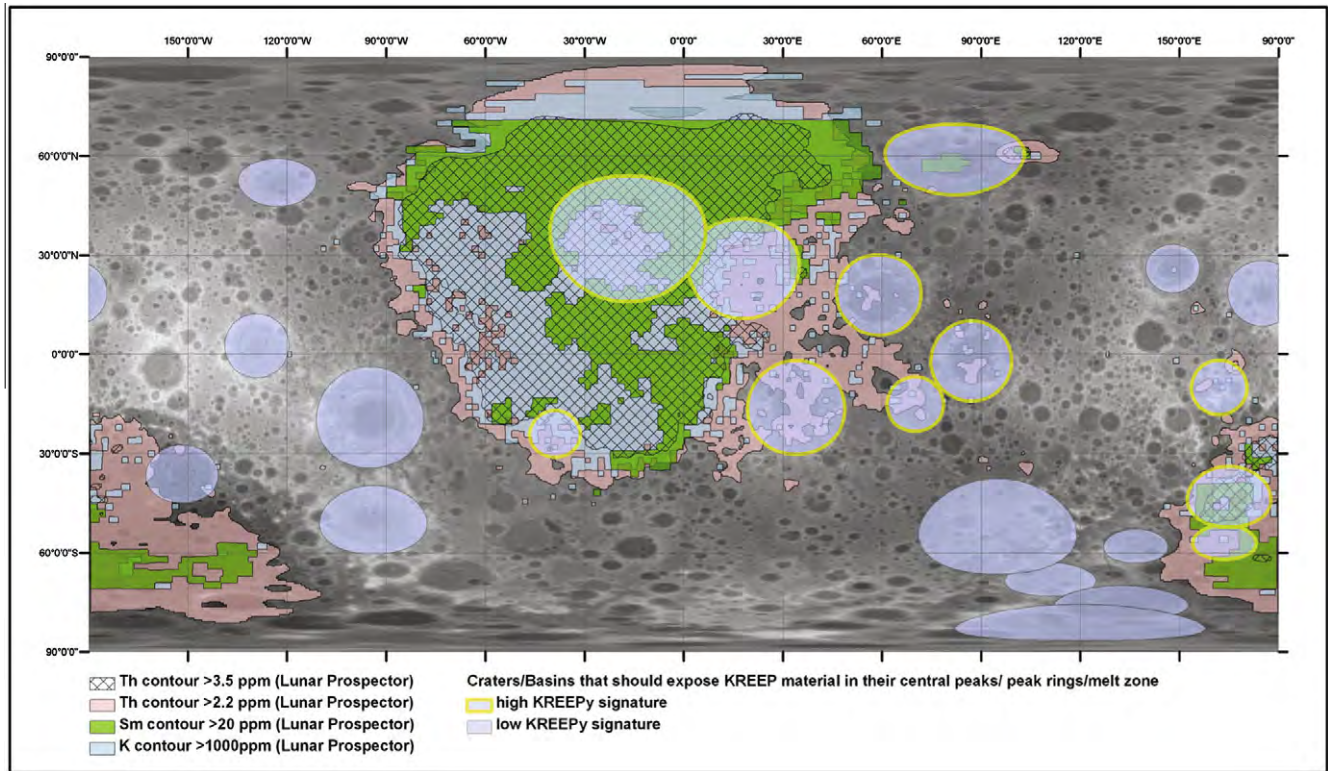


Fig. 4. Distribution of craters or basin sampling a hypothetical global urKREEP layer (based on calculations), compared to contours depicting enriched abundances of thorium, potassium, and samarium. Sites with a KREEPy signatures are highlighted with a yellow outline.

help locate the main geochemical terranes (Jolliff et al., 2000) and possible regional anomalies. In relation to NRC report concept 3, these maps are useful for understanding lateral heterogeneities in crustal composition. Of particular interest are maps depicting the abundances of thorium (Th), samarium (Sm), and potassium (K). Elevated concentrations of these incompatible elements are taken to be indicators of the presence of KREEP-rich material (Snyder et al., 1995; Gillis et al., 2004; Wiczorek et al., 2006). Thorium enrichment is defined at abundances  $>2.2$  ppm, while regions containing over 3.5–4.5 ppm are almost entirely located in the mare regions of the nearside (this region, generally labeled the Procellarum KREEP Terrane (PKT) is discussed further in Section 3 of this paper and in Haskin et al. (2000) and Jolliff et al., (2000)). We created contour maps depicting the areas of the lunar crust that are enriched in thorium ( $>2.2$  ppm and  $>3.5$  ppm). Similarly, we computed contour maps for samarium abundances greater than 20 ppm, and potassium abundances greater than 1000 ppm (Jolliff et al., 2000; Elphic et al., 2000). It should be noted that the Lunar Prospector potassium data are less reliable due to their low spatial resolution of  $5^\circ$  per pixel.

We mapped different surface units on the Moon and digitized them in the form of vector outlines or shapefiles. These mapped surface units include: mare areas, cryptomare areas, highland areas, highland types (based on Chevrel et al., 2002), basin areas, pyroclastic (based on Gaddis et al., 2000, 2003) and other volcanic deposits, as well as

fresh craters (Copernican and bright-rayed from Werner and Medvedev (2010)).

To assess the vertical structure of the lunar crust, we calculated morphological parameters related to impact cratering, including the depth of excavation and maximum depth of melting (cf. Section 2.2). Maps depicting the global variations of these parameters were created and added to the GIS. All of the aforementioned maps were combined and overlaid to help evaluate different potential lunar landing sites. All maps presented in this paper were registered using the Moon\_2000 coordinate system in the Plate\_Carree (equidistant cylindrical) projection.

## 2.2. Proximity models

In the context of NRC report concept 3, the selection of lunar landing sites requires knowledge of locations on the Moon's surface where material originally formed in the (deep) lunar subsurface might be exposed. To locate such sites, we used an approach developed by Wiczorek and Zuber (2001) and Cahill et al. (2009) for determining the possibility of sampling material from the upper crust, lower crust or mantle at an impact crater's location. This approach is based on an indirect method of quantifying the vertical and lateral heterogeneity of the lunar crust by considering impact craters as natural drills that sample material from layers deep within the Moon's interior. Large complex impact craters and impact basins have the capacity to excavate or uplift material from the lower crust and

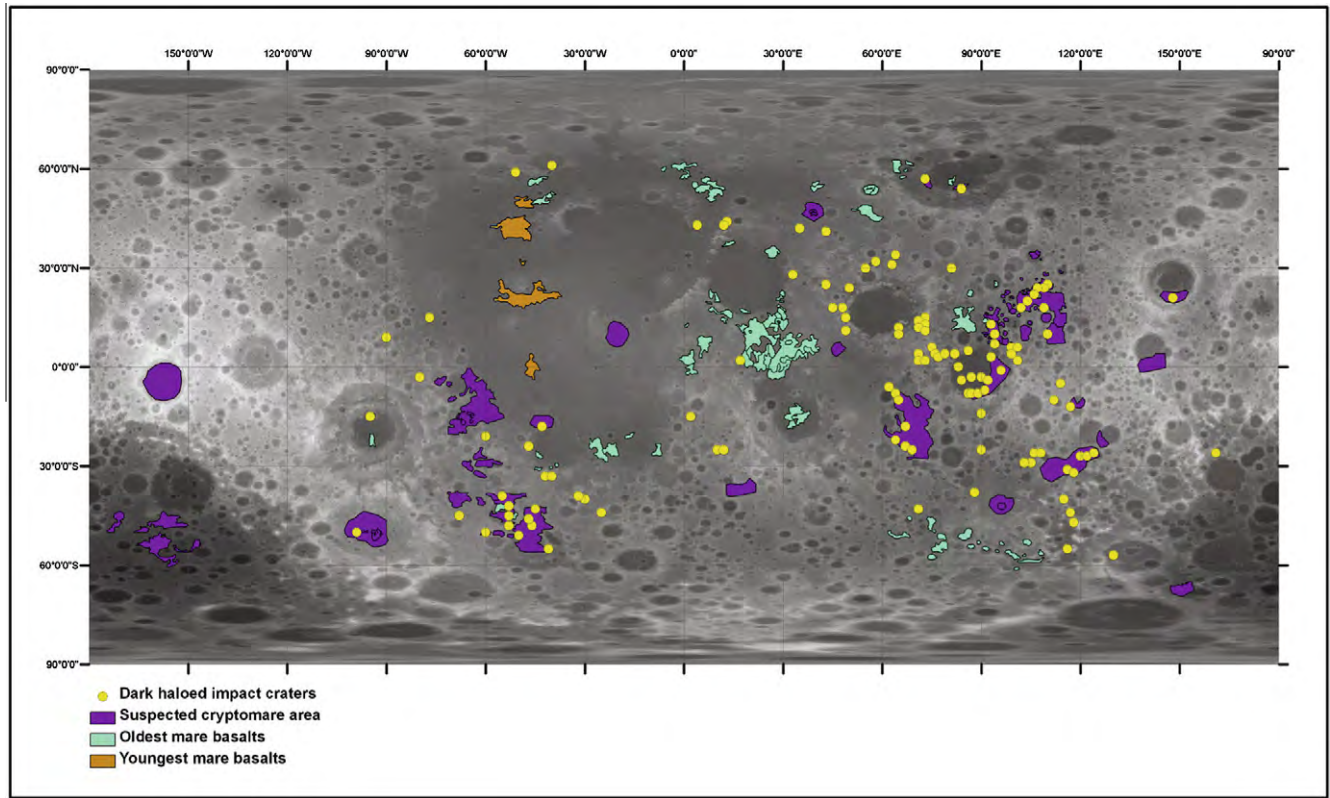


Fig. 5. Combined map showing the location of the oldest and youngest known mare basalts, as well as possible areas of cryptomare (List in Appendix D), usually identifiable with dark haloed craters or mixed signatures. Estimated surface ages of mare basalts were based on crater counts (map compiled using the data of Tyrle, 1988; Greeley et al., 1993; Neukum and Ivanov, 1994; Hiesinger et al., 2000, 2003, 2006, 2008; Haruyama et al., 2009) and general distribution of dark-haloed impact craters larger than 1 km in diameter determined by Schultz and Spudis (1979).

upper mantle. We examined all the complex craters and impact basins listed in the Lunar Impact Crater Database (Losiak et al., 2009; revised by Ohman at LPI) to determine where on the Moon that material might be found.

### 2.2.1. Calculations of relevant morphological parameters

**2.2.1.1. Excavation depth.** Depth of excavation refers to the maximum depth of origin of crater ejecta. Target material deeper than the maximum depth of excavation is displaced downward beneath the crater floor, and does not emerge in the ejecta to be deposited on the target's surface. Strata below the depth of excavation are thus pushed downward (Melosh, 1989). Using the Maxwell Z-model for excavation flow (Maxwell, 1977) and assuming a 45° impact angle for  $Z = 3$ , the maximum depth of excavation ( $D_e$  in km) is found to be about 1/3 of the final transient crater depth ( $D_{td}$  in km) or about 1/10 of the final transient crater diameter ( $D_{tc}$  in km), as shown in Eq. (1) below (Melosh, 1989; Croft, 1980).

$$D_e = D_{td}/3 = D_{tc}/10 \quad (1)$$

For complex craters, we utilized Eq. (2) (all units in km) to find the transient diameter  $D_{tc}$  (Croft, 1985; Cintala and Grieve, 1998). Here,  $D_{sc}$  is the transition diameter from simple to complex craters (approximately 16–20 km for the Moon), and  $D$  the final rim diameter

$$(D_{tc} \cdot 10^{-5})^{1.18} = (D \cdot 10^{-5}) / (D_{sc} \cdot 10^{-5})^{-0.18} \quad (2)$$

**Depth of melting.** We calculated the depth of melting ( $D_m$ ) corresponding to each crater to determine if the mantle and/or lower crust are chemically represented in the melt emplaced at the surface by the impact event. We also used  $D_m$  to determine the depth of material that might be exposed in central peaks, assuming the maximum depth of melting is equal to the minimum depth of origin for central peaks (Cintala and Grieve, 1998). Eq. (3), based on impacts of chondritic projectiles into anorthosite at 16.1 km/s, was used to calculate  $D_m$  corresponding to each crater (e.g., Cahill et al., 2009; Tompkins and Pieters, 1999).

$$D_m = 0.109D^{1.08} \quad (3)$$

Eqs. (1)–(3) were derived for complex central peak to peak ring craters and are assumed here to be valid for basin-size structures too.

### 2.2.2. Determination of average pre-impact lunar crustal thickness

To determine if the material excavated by a crater originated from the lower crust and/or mantle, analyses of individual craters were combined with models of crustal thickness. In this study, we used crustal thicknesses derived from models based on Clementine topography and Lunar

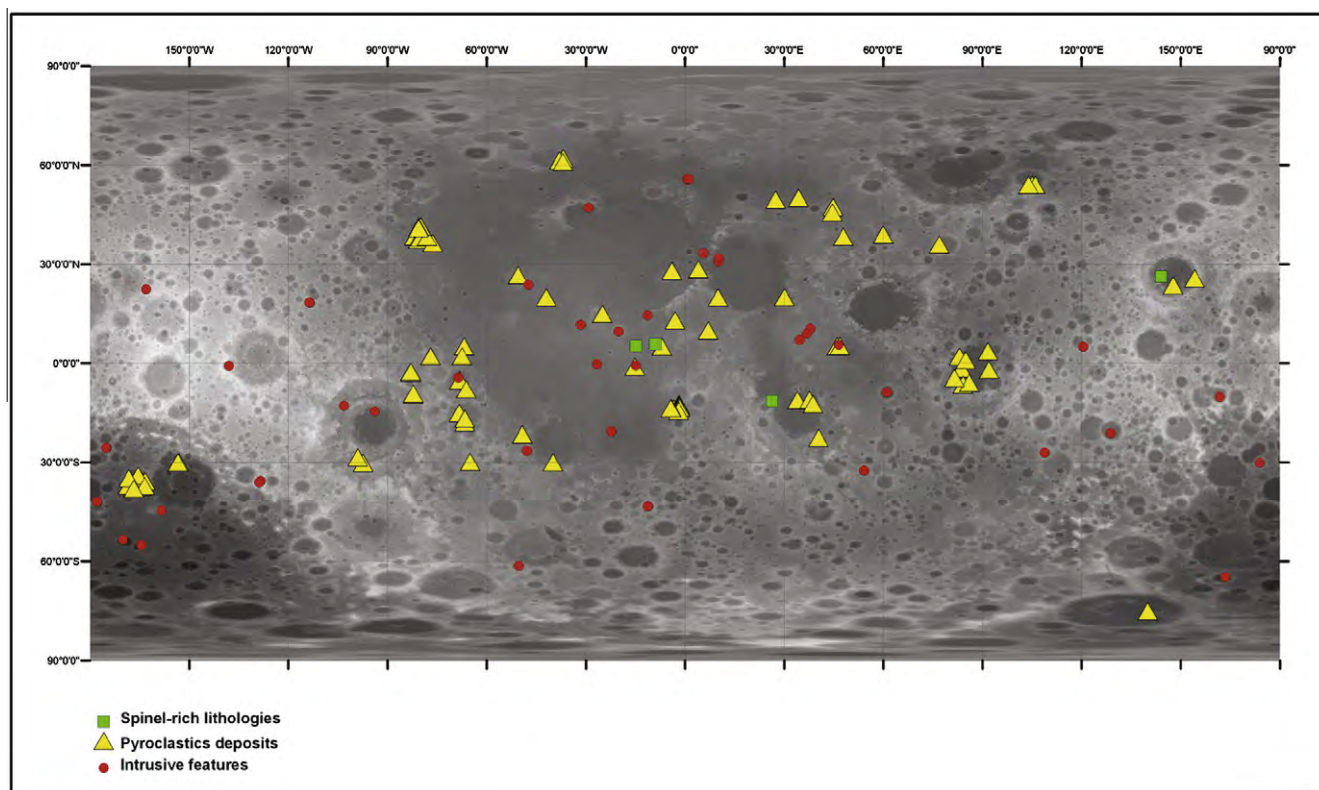


Fig. 6. Combined map of potential lithologies of interest that need to be sampled within their geological context: spinel (from Pieters et al. (2010), Sunshine et al. (2010) and Dhingra et al. (2011)), pyroclastics (List in Appendix E), and various intrusive features reported in the literature (List in Appendix F).

Prospector gravity data (Wieczorek and Phillips, 1998; Wieczorek et al., 2006). These models may be inaccurate for the far side because of the lack of farside gravity coverage, and our analysis should be repeated when more accurate crustal thickness estimates based on Kaguya or GRAIL data become publicly available. Wieczorek and Phillips (1998) considered two single-layered models and one dual-layered model; we took into account estimates from all three models. The crustal thickness values reported in these models represent present-day values. We instead require an estimate of the pre-impact crustal thickness to accurately evaluate crust-mantle materials affected by the impact events. To calculate the average pre-impact crustal thickness corresponding to each crater in the Lunar Impact Crater Database, we took an average of the crustal thickness values corresponding to an annulus of pixels located at a distance equal to one crater diameter from the rim  $\pm 10\%$  of the crater diameter.

### 2.2.3. Determination of source of material in ejecta blanket/central peak/melt sheet

We compared the excavation depth and the maximum depth of melting with the crustal thickness at each of the crater locations to determine if material in the ejecta blanket/central peak was derived from the upper crust, lower crust, or the mantle (similar to the calculations performed by Cahill et al. (2009) (Fig. 1). The difference between the

estimated pre-impact crustal thickness and the calculated depth of excavation or depth of melting is labeled 'proximity'. If this proximity value is positive, then the crustal thickness is greater than the impact depth reached, and material from below the crust is not exposed at the surface. If the calculated proximity has a negative value, the impact exposed material from below the crust/mantle boundary. To increase the reliability and accuracy of our results, we applied a down-sampling criterion to the returned proximity values. Any crater with a proximity value greater than -5 km was not taken into account, as it would be within the modeling technique errors. Although these proximity calculations are mostly used to study the crust/mantle interface, they can also be applied to the upper crust/lower crust interface by taking into account the thickness estimates for the upper crust only (based on Wieczorek and Phillips (1998) dual-layered model). This would indicate where lower crust material could have been exhumed on the lunar surface (with a similar 5 km error bar).

It should be noted however that our calculations do not take into account the smaller, more recent craters that might have exposed the older impact melt of large basins. If these craters are too shallow to reach the crust-mantle boundary (or the upper crust-lower crust boundary), they would not be identified through our calculations as sampling mantle/lower crust material, even though they might be penetrating through the melt of the basin.

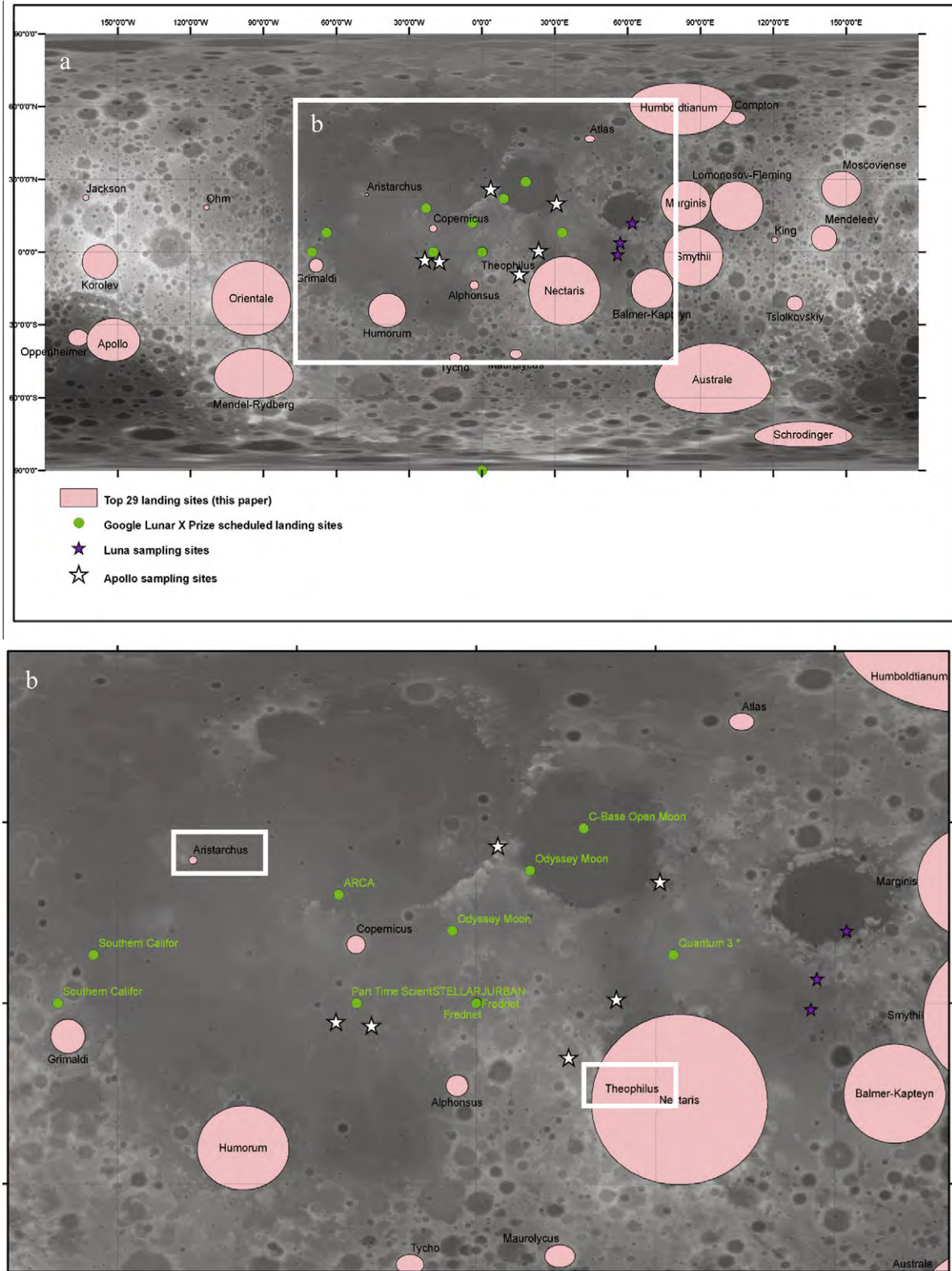


Fig. 7. Map displaying our 29 top landing sites, compared with the preliminary landing sites scheduled for the GLXP future lunar missions. White and purple arrows respectively indicates Apollo and Luna landing sites that led to the return of samples to Earth. B is a close-up on the nearside of the Moon, close to the equator, showing possible regions of interest nearby the proposed GLXP landing sites.

### 3. Landing sites selection for NRC report goals 3A and 3B

#### 3.1. Definition of goals and scientific background

Concept 3 of the NRC report is divided into five sub-goals, two of which feature in the top 11 overall science priorities: (3A) ‘Determine the extent and composition of the primary feldspathic crust, KREEP layer and other products of differentiation’ and (3B) ‘Inventory the variety, age, distribution and origin of lunar rock types’.

Goal 3a relates to constraining the vertical stratigraphy of the lunar crust and to the products of interior differentiation in the context of the lunar magma ocean (LMO) model. Assuming the Moon was completely molten to a depth of hundreds of kilometers right after its accretion (e.g., Wood et al., 1970; Shearer et al., 2006), the existence of a magma ocean at the surface is thought to have had a major impact on lunar differentiation and evolution. Progressive crystallization of the cooling magma ocean would have led to a stratified interior, with early-formed, dense cumulates containing olivine and pyroxene sinking to the bottom of the ocean, and lighter material including plagioclase-rich cumulates floating to the top, forming the upper crust (e.g., Warren, 1985; Spudis and Davis, 1986; Snyder et al., 1992). This process also triggered an inhomogeneous vertical distribution of minor and trace elements. The last remaining liquid to crystallize, known by the term urKREEP, was significantly enriched in heat-producing and incompatible elements including potassium (K), rare earth elements (REE) and phosphorus (P) (Warren and Wasson, 1979) (the ur- prefix means “original” or “primitive”, and is used specifically to distinguish the incompatible-rich layer that formed through the LMO from secondary KREEP-rich material). Although this concept has served well since the days of the Apollo missions, remote sensing, geophysical measurements, and sample analysis reveal that the lunar crust is not simply vertically stratified, but also varies laterally. The lunar surface seems to consist of multiple geologically distinct provinces that may be the result of internal or external processes, or a combination of both. Examples of such processes include spatial variations in tidal heating (Garrick-Bethell et al., 2010), asymmetry in the crystallizing lunar magma ocean (e.g., Jolliff et al., 2000; Elkins-Tanton et al., 2011), asymmetric cratering (Wood, 1973), and late accretion of a companion moon (Jutzi and Asphaug, 2011). To improve our understanding of the evolution of the Moon, it is important to determine the composition and the spatial extent of each of the main differentiation products: the primary feldspathic crust, the urKREEP layer, and the mantle (Warren and Wasson, 1979).

The aim of Goal 3b is to catalogue the surface products of all types of planetary processes by identifying all rock types present on the lunar surface. As stated above, the lunar crust exposed at the surface varies in composition, age, and mode of emplacement, a fact that the LMO model cannot easily account for (e.g., Jolliff et al., 2000, 2011).

The Apollo samples, which originate from a limited proportion (<4%) of the lunar surface area of the Moon (Warren and Kallemeyn, 1991), revealed a variety of rock types (e.g., Shervais and Taylor, 1986). Some of these rocks were expected (such as basalts), and some varieties were unexpected, such as the occurrence of granites (Ryder, 1976). Some key hypothesized rock types, including pristine anorthositic crust, urKREEP, and mantle material, are absent in our sample collection, even when lunar meteorites are taken into account (e.g., Warren, 2005). In addition, remote sensing data suggest some smaller unsampled regions contain unique materials that can be of great interest to both fundamental and applied lunar science (e.g., the recent discovery of spinel-rich outcrops by M<sup>3</sup>, Pieters et al., 2010). Compiling a database of all the lunar rock types and their age as suggested by Goal 3b is crucial to understand the history and evolution of the Moon.

#### 3.2. Requirements

For each goal, we suggest a list of requirements that are used to identify optimal landing sites. The four main requirements for targeting potential landing sites that may accomplish Goal 3a are suggested to be:

- A1. Target sites with the potential to yield representative samples of planetary differentiation products missing from our current sample collection (e.g., primordial anorthositic crust, lower crust, urKREEP, mantle).
- A2. Target sites that could demonstrate the variety of lunar highlands mineralogy and composition.
- A3. Target sites that will allow sampling of the 3 main geochemical terranes (Jolliff et al., 2000): (Feldspathic Highlands Terrane, FHT; Procellarum KREEP Terrane, FHT; South Pole Aitken Terrane, SPAT).
- A4. Target sites that enable determination of the spatial extent and composition of the urKREEP layer.

We suggest the following three main requirements for identifying optimal landing sites for accomplishing Goal 3b:

- B1. Target multiple sites that provide samples cataloging the chronological history of the Moon, using crater density determined from remote sensing as an approximation of rock age.
- B2. Target sites likely to provide samples cataloging the lithological diversity of lunar rocks.
- B3. Target sufficient sites to collect samples from all of the main regions of the Moon.

As described below, we mapped relevant features for each of these seven requirements and identified sites where multiple requirements could be addressed in a single mission. The resulting list of potential landing sites was ranked according to the number of requirements they could meet.

Two of the most promising sites are discussed in more detail in Section 4.

### 3.3. Selected landing sites related to Goal 3a

#### 3.3.1. Landing sites meeting requirement A1

The best sampling sites were determined for each of the main LMO differentiation products, and then integrated to identify the best overall landing sites meeting requirement A1.

*Primordial feldspathic highlands material.* The primary feldspathic crust is expected to be a ferroan-rich anorthosite, with very high and nearly pure plagioclase content (Warren and Wasson, 1977, 1979; Pieters, 1986; Taylor, 1982; Wiczorek et al., 2006). Sites to investigate include the highland areas and the recent purest anorthosite (PAN) detections. PAN was detected by Earth-based instruments as well as remote-sensing instruments onboard various spacecraft (Fig. 2, Appendix B) (Hawke et al., 2003a; Tompkins and Pieters, 1999; Ohtake et al., 2009, 2010). PAN detections are abundant in almost all fresh craters larger than 30 km in diameter, prompting the hypothesis that there might be a ubiquitous PAN layer buried under the mixed and brecciated surface material, especially in the highland areas (Hawke et al., 2003a; Ohtake et al., 2009). This PAN layer might represent remnants of the ancient upper crust formed from the LMO. The lunar highlands are expected to contain feldspathic material derived from the ancient upper crust. However, recent studies of the feldspathic highlands (Chevrel et al., 2002; Nyquist et al., 2010) suggest that not all highlands material is derived from the LMO; other formation processes may have led to various highland types. Chevrel et al. (2002) identified and mapped at least 5 highland types; the types ‘H1’ and ‘H2’ that are abundant in the FHT as defined by Jolliff et al. (2000) may correspond to the most pristine highland material (cf. Section 3.3.2). Sampling H1 and H2 material in their original geological context would consequently be highly valuable and could be achieved in young craters impacting those highland types which could contain fresh outcrops.

*Lower crust, urKREEP and mantle material.* As the lower crust and mantle layers should not typically be exposed on the lunar surface, the best way to observe material from depth is through impact cratering processes (e.g., Tompkins and Pieters, 1999). There are three locations in the vicinity of an impact crater where this material could be sampled: the ejecta, the central peak (or peak rings), and the melt sheet. We determined where on the surface of the Moon the lower crust, urKREEP layer or mantle could be sampled by comparing impact excavation depth and melt depth to estimated crustal thickness as described in Section 2.2 (Appendix A). Excavation depth provides information on the depth of origin of ejecta material. Conversely, melt depth estimates the depth of origin of material contained within impact melt, and also provides a minimum limit to the depth of origin of the uplifted central

peak/peak ring material. We suggest that central peaks or rings might represent better sampling sites as they likely expose rocky outcrops, but a list of crater ejecta in which lower crust or mantle material should be present is also given in Appendix A. Results show that there are hundreds of craters that could have tapped into the lower crust, containing some of this material in their melt sheet or central peaks; on the contrary, less than 40 craters might contain mantle material in their melt or peak rings (Fig. 2, Appendix A). As the urKREEP layer is expected to have been sandwiched between the lower crust and mantle (Warren and Wasson, 1979), all basins excavating mantle material should also have excavated urKREEP material, assuming the urKREEP layer is globally distributed (the case of a possible patchy urKREEP layer is discussed in Section 3.3.4). LOLA data were used to determine which of these craters or basins have preserved central peaks or peak rings, and can be considered as good sampling sites. Recent olivine detections from the SELENE/Kaguya mission (Yamamoto et al., 2010) were also considered as they provide possible evidence for mantle outcrops.

Final science-rich mission sites meeting requirement A1 are mapped on Fig. 2. Assuming a 10–20 km traverse range for a mission on the lunar surface, our analysis shows that in general, impact craters and especially central peaks, are the best locations to study the main LMO differentiation products absent from our current sample collection. It is also clear that there is no single location where all main LMO differentiation products can be sampled at once. Analyzing and/or collecting representative samples of each of the differentiation products thus implies multiple landings at different sites.

#### 3.3.2. Landing sites meeting requirement A2

As mentioned above, Chevrel et al. (2002) divided the highlands areas into at least five compositional types using data from instruments onboard Clementine and Lunar Prospector spacecrafts. Highland samples are rare in the Apollo collection, and correspond mainly to highland types H3 and H5, which are thorium-rich units influenced by the urKREEP layer.

Since the highlands are generally very old and have been superficially mixed, brecciated, and covered by regolith, particular care must be taken when selecting locations to land within the highlands. Locations with fresh exposures of highland material are preferred; we therefore suggest using the fresh craters emplaced on the highlands types H1–H5 of Chevrel et al. (2002) (Fig. 3, Appendix C). Young (*i.e.* Copernican) and rayed crater (bright rays are an indicator of young age) (Werner and Medvedev, 2010) locations were projected on top of the highland variety map of Chevrel et al. (2002), and craters impacting different highland-type compositions were marked (Fig. 3). A list of these craters is provided in Appendix C. H1 and H2 sites, which might represent the most pristine anorthosite crust, should be targeted to meet requirement A2, but a sample of the H4 type would be useful too.

### 3.3.3. Landing sites meeting requirement A3

Fig. 3 shows a map of the three main geochemical terranes, generated based on the criteria defined by Jolliff et al. (2000) (Fig. 3):

The Procellarum KREEP Terrane (PKT) area is bound by the thorium 3.5 ppm ( $\mu\text{g/g}$ ) contour line.

The South Pole-Aitken Terrane (SPAT) area has iron abundances larger than 5 wt% (up to 8 wt% in the inner SPAT).

The Feldspathic Highland Terrane (FHT) is divided into two areas: the FHTa, which corresponds to the farside highlands where the crust is thicker than 70 km, and the FHTb which corresponds to everything outside all of the previously defined parameters.

Analyzing representative samples from each of the individual terranes can essentially be fulfilled by landing anywhere within the three distinct provinces. As a result, the optimal landing sites within these terranes should be selected on the basis of their also fulfilling other requirements.

### 3.3.4. Landing sites meeting requirement A4

The urKREEP layer corresponds to the last liquid that crystallized from the LMO. Although it occupies <1% of the lunar magma ocean by volume, urKREEP is thought to have contained about half of the Moon's incompatible elements (Warren and Wasson, 1979), and as a result forms a crucial part of the LMO model. Results from missions such as Lunar Prospector and Clementine have questioned the global extent of this hypothesized layer (Jolliff et al., 2000). Contrary to the early model of a uniformly distributed urKREEP layer, current observations of patchy incompatible element abundances on the lunar surface may suggest an asymmetrical distribution of urKREEP (Wieczorek et al., 2006), making it a regional attribute of the PKT region (e.g., Wieczorek and Phillips, 2000; Parmentier et al., 2002). Furthermore, Yamaguchi et al. (2010) recently determined that there was not a KREEP component in the genesis of anorthosite and basaltic clasts within lunar meteorite Yamato-86032, which implied the meteorite came from a region far from the PKT, such as the lunar farside, and that an urKREEP horizon did not underlie that part of the Moon.

The hypothesized, primordial urKREEP layer of the LMO has not been sampled directly. It is inferred from extensive analyses of Apollo samples, which contain basalts that entrained a KREEP component. KREEP basalts are thought to originate in the deep lunar mantle and assimilate part of the urKREEP reservoir on their way to the surface (e.g., Warren and Kallemeyn, 1998). It would, thus, be interesting to locate outcrops where that urKREEP layer can be sampled directly.

Using the previous proximity calculations (Sections 2.2 and 3.3.1), we identified areas where models indicate excavation or melting of mantle material, and therefore

possible urKREEP presence. In Fig. 4, blue circles depict craters or basins that could have uplifted material from the urKREEP layer in their central peak or incorporated it into their impact melt. As urKREEP material is expected to be enriched in incompatible elements such as Th, Sm and K, we compare the selected craters to the enrichment contour maps of these elements. In the case of a global urKREEP layer, the identified craters should all show geochemical evidence of KREEP either in their central peak or within the melt sheet. Fig. 4 shows that not all of the craters show high KREEP signatures. This may confirm a patchy lateral extent of the urKREEP layer, in support of heterogeneous urKREEP models (e.g., Parmentier et al., 2002; Wieczorek et al., 2006). However, we cannot discount the possibility that the features are covered by layers of regolith or mare basalts, hiding the urKREEP signature. For this reason, we suggest that any sites located outside the boundaries of PKT with a high KREEP signature could provide representative samples of KREEP-rich, and possibly urKREEP material (e.g., the northern rim of Compton crater; Antoniadi crater in SPAT). Craters that penetrate the urKREEP layer in the proximity model, yet show no KREEP signatures are also science-rich target sites. Such craters are of interest to explore the patchy nature of urKREEP, and to identify which rocks form the crust-mantle boundary if not a layer of KREEP-rich material.

## 3.4. Selected landing sites related to Goal 3b

### 3.4.1. Landing sites meeting requirement B1

The Apollo samples showed that most lunar rocks are very old compared to terrestrial rocks, and that their ages span a wide range from >4 Ga to < 3 Ga (e.g., Nyquist et al., 2001 and references therein). Crater density analyses (e.g., Hiesinger et al., 2008) suggest that some surface rocks could be as 'young' as 1 Ga, but to date no lunar samples have yielded this young age. The oldest lunar rocks are likely to be the products of LMO differentiation, as described in requirement A1. Other sites of interest include locations showing evidence for geological activity after the end of LMO crystallization, for example areas containing products of serial magmatism that would enable the characterization of the primitive lunar mantle after the completion of LMO crystallization.

Mare basalts, which are thought to be formed by ancient volcanism, cover about 16% of the lunar surface, the majority of which is exposed on the lunar nearside (Wilhelms, 1987). Basalts vary in terms of age, elemental and isotopic composition (e.g., titanium content), and mineralogy. Sampling the youngest and oldest mare basalts is required to understand how volcanic processes varied as a function of time. Fig. 5 shows the latest results for mare dating based on crater counting, which highlights the fact that lunar volcanism was active over a long period of time, starting at ~4 Ga and ending at ~1.1 Ga (Hiesinger et al., 2008). The youngest basalts appear to be located in

Oceanus Procellarum, in the vicinity of the Aristarchus Plateau, while very old mare basalts are preferentially located within Mare Tranquillitatis, Mare Australe, Mare Marginis, Mare Humboldtianum, Mare Orientale and Mare Humorum.

The oldest mare basalts, termed ‘cryptomare’ (plural, ‘cryptomaria’) (e.g., Schultz and Spudis, 1979; Antonenko et al., 1995), are widely considered to be buried and obscured from view by subsequent emplacement of material of higher albedo, commonly ejecta from craters and basins. Cryptomaria are primarily detected by the presence of dark-haloed craters – later formed impact craters that penetrated the outer regolith layer, ejecting the darker mare material that lies underneath. Evidence for the old age of cryptomare is mostly in the form of stratigraphic relationships, as many cryptomaria are suspected to underlie material as old as pre-Nectarian in age (Hawke et al., 2005a). Cryptomare basalts have not been sampled yet, although the lunar meteorite Kalahari 009 has been interpreted to be a sample of cryptomare. Kalahari 009 has been radiometrically dated at  $\sim 4.35$  Ga and shows extremely low abundances of incompatible elements including thorium and the rare earth elements (Terada et al., 2007). Cryptomaria may represent the oldest mare volcanism on the Moon, and could convey information on the mantle and early volcanism, and their temporal evolution.

Fig. 5 shows the general distribution of dark-haloed impact craters larger than 1 km in diameter as determined by Schultz and Spudis (1979), and the locations where cryptomare areas have been detected (Bell and Hawke, 1984; Pieters et al., 2001a,b; Antonenko, 1999; Antonenko and Yingst, 2002; Hawke et al., 2003b, 2005a,b; Giguere et al., 2003, 2007; Campbell and Hawke, 2005, see compilation in Appendix D). We note that both the dark-haloed craters and the cryptomaria presented here do not constitute a comprehensive list, as many potential cryptomare sites may still be unidentified (Antonenko, 1999). Apart from the cryptomaria mapped in the regions of Lomonosov-Fleming, Balmer-Kapteyn, Schiller-Schickard, SPA, and the South–West margin of Procellarum (which have been studied in detail), all the other contours are very imprecise and should only be taken as approximate locations of cryptomare. Fig. 5 also maps the units that have been interpreted as being mixtures between highlands and mare materials by Chevrel et al. (2002), with 6.6–7.8 wt% in Fe, 0.15–0.35 wt% in Ti and 1.1–1.5 ppm in Th. These locations correspond mostly to cryptomare deposits detected using other methods, and thus add evidence for their presence in these parts of the Moon.

### 3.4.2. Landing sites meeting requirement B2

This section focuses on the different lithologies that are of high scientific interest and were not already investigated in Goal 3a (Section 3.3).

*Mare basalts.* The integration of global maps of thorium, iron and titanium abundances led to a subdivision of the lunar maria in five types, named M1–M5 (Chevrel

et al., 2002). M1 and M2 are high-titanium mare basalts, with differing thorium contents, while M3 and M4 units are less enriched in titanium, again with different thorium contents. M5 is the only unit with very low titanium levels, and the lowest iron content as well. The mare rocks gathered during the Luna and Apollo missions mainly represent M1, M3 and M4 types, although this evaluation remains quite imprecise. M2 and M5 types are lacking in the sample collection, and sampling and analyzing them could greatly improve our knowledge on the variety of mare rock types. As it is still uncertain whether farside magmas were derived from a similar source and depth as the nearside basalts (Wieczorek et al., 2006), sampling both farside and nearside mare basalts also appears recommendable.

*Pyroclastic deposits.* “Fire-fountain” eruptions have left pyroclastic deposits (quenched iron-bearing glass and crystallized beads with volatile-element coatings that have chilled from the spray of molten lava) on the surface (Lucey et al., 2006). Sampling pyroclastics is interesting as the pyroclastic glasses identified in the Apollo samples are primitive and hence provide among the best views of interior source compositions. Most of these deposits are of late Imbrian age, generally 3.2–3.7 Ga, corresponding to the age of the peak period of ancient lunar volcanism (Gaddis et al., 2003). Fig. 6 (and corresponding Appendix E) shows that pyroclastic deposits are widely distributed on the whole surface of the Moon; they can also greatly differ in terms of both spatial extent (from 1 km<sup>2</sup> to 49,000 km<sup>2</sup>) and composition.

*Intrusive features.* Compositional and petrographic relations among the lunar samples suggest that unmapped plutonic activity contributed significantly to early crustal evolution. Plutons might have been formed early after the magmatic ocean crystallized by intense and repeated periods of serial magmatism. Remote sensing study of Bullialdus crater (21°S, 22°W) showed the possible existence of a pluton at this site, whose size was estimated to be on the order of the size of the crater ( $\sim 60$  km) (Pieters, 1991). Based on the character of mafic minerals present and compositional diversity with depth, most additional candidate areas for pluton excavation appear concentrated in the western hemisphere: for instance Copernicus, Aristarchus, and Tycho (Pieters, 1991). Seven highland craters (namely Jackson, King, Langmuir, Orlov, Ohm, Stevinus and Tycho) in which the central peaks are more mafic than the central peaks of other highland craters, were identified using Clementine UVIS data (Tompkins, 1998). These seven mafic craters are not supposed to have tapped the deeper mafic lower crust; their particular composition can reasonably be interpreted by the occurrence of excavated plutons at these locations. Plutonic rocks exhibit a range of compositions that include dunites, troctolites, norites, and gabbro-norites, although anorthosite-rich plutons may also exist on the Moon. For example, Nyquist et al. (2010) identified highland material that had a different age and isotopic composition than the primordial highlands formed from the LMO. Similarly, Borg et al. (2011)

also recently reported the existence of 4.36 Gy ferroan anorthosites.

Unfortunately, plutons are hard to identify as their composition might be similar to the composition of the upper (in the case of anorthosite-rich plutons) or lower (in the case of mafic plutons) crust. The only ways to distinguish them from the material of the primordial crust formed by the magma ocean, is by their geological context (*e.g.*, outcrops in central peaks of small craters that are only reaching the subsurface material, intrusive contacts in crater walls or cliffs). Rocks formed in plutons will have a different age and isotopic composition from those of the rocks formed from the magma ocean, as they have different formation processes, but these parameters cannot be assessed with remote sensing data or in situ measurements at present – as a consequence it will be crucial to return samples of plutonic intrusions to the Earth to date plutonic activity.

Other intrusive features include subsurface magmatic intrusions, where magma flows under a surface of solidified lava and lifts it up, forming flattened or domical shaped features. Such features on the Moon are called intrusive domes. Intrusive domes do not display effusive vents and differ morphologically from the common effusive domes. They are characterized by very low flank slopes of less than  $0.9^\circ$ , often have larger diameters than effusive lunar domes (30 km and more), and display regular but non-circular outlines (Wöhler and Lena, 2009). These domes tend to be associated with tectonic faults or linear rilles, which are indicative of tensional stress and may suggest their possible intrusive mode of formation. Wichman and Schultz (1996) attributed the modification processes observed in floor-fractured lunar craters to the formation and growth of laccoliths.

These intrusive features are also hard to locate with remote sensing data, especially since high resolution gravity data have not been publicly released yet. Still, an attempt to map some of these features was made in Fig. 6 which presents probable locations of intrusive material exposures, namely plutons, laccoliths, and intrusive domes that were reported in the literature (list in Appendix F). Visiting these sites would help understand the complexity of the current lunar crust on a local scale.

*Spinel-rich lithologies.* Spinel group minerals are common in lunar samples, but only occur as accessory phases (modal abundances of  $<10\%$ ). Investigation of spectral anomalies in global data acquired with the Moon Mineralogy Mapper ( $M^3$ ) onboard the Chandrayaan-1 mission revealed a spinel-rich lithology on the central nearside, found among the Sinus Aestuum pyroclastic deposits ( $5.1^\circ\text{N}$ ,  $15.2^\circ\text{W}$  and  $6.0^\circ\text{N}$ ,  $8.4^\circ\text{W}$ ), thus consistent with a volcanic origin, but notably absent from the adjacent Rima Bode pyroclastic deposits ( $12.0^\circ\text{N}$ ,  $4.1^\circ\text{W}$ ) (Sunshine et al., 2010). While the pyroclastic deposits are spatially extensive ( $\sim 10^4 \text{ km}^2$ ), the spinel-rich signatures occur at much smaller scales ( $<1 \text{ km}$ ). A possible explanation for the presence of these spinel-rich deposits is that they may have been underlying the thin layer of pyroclastic glass deposits, and were exposed by subsequent cratering of the region.

The observation that the whole region is embayed by mare volcanism with the spinel-rich and pyroclastic deposits exposed only on topographic highs suggests that the spinel-rich deposits are ancient (Sunshine et al., 2010).  $M^3$  data also allowed the detection of a rock type dominated by Mg-rich spinel with no other detectable mafic minerals on the western edge of Mare Moscoviense, as well as in the central peak of Theophilus crater (Pieters et al., 2010; Dhingra et al., 2011). These detections do not easily fit with current crustal evolution models and has been interpreted as being a new, unsampled rock type. Sampling and analysis of spinel-rich lithologies could bring new insight into early lunar volcanism and help to constrain lunar evolution models.

*Impact rocks.* Breccias are clastic rocks composed of pieces of older rocks that were disaggregated or melted by meteoroid impacts, and subsequently lithified. Different types of breccias should occur near an impact structure, depending on where they formed (Stöffler, 1981). Given the variety of compositions that can be displayed in breccias (according to the crater age, size, and excavation depth), we suggest that samples coming from various locations in and around an impact crater are needed to get a representative breccia types sample collection. Precise cataloging of the all types of impact-related breccias would improve our understanding of cratering processes. Access to impact rocks can be achieved at virtually any crater site on the Moon. Fig. 6 provides a compilation of all features of interest we identified for addressing requirement B2.

#### 3.4.3. Landing sites meeting requirement B3

Requirement B3 implies multiple sampling sites on various locations on the Moon. Although all sample return missions to the Moon would contribute to fulfilling part of this requirement, some sites are scientifically richer than others. For instance, even though nearly all the different lithologies of the lunar crust can be found mixed together in the regolith (usually in a brecciated form), information regarding their respective geologic contexts are lost in this case. We suggest that optimal sampling sites should be selected by integrating all features of interest listed in the other two requirements of Goal 3b (Fig. 5 and 6).

### 4. Selected landing sites meeting goals 3A and 3B

A complete list of considered landing sites for each goal is available in Appendix G. We note that no single location can fulfill all the requirements for Goal 3a, nor can a site be identified that meets all requirements for Goal 3b. The top ten landing site candidates are the Orientale basin, Schrodinger basin, Apollo basin, Aristarchus crater, Australe basin, Copernicus crater, Humboldtianum basin, Humorum basin, Korolev crater, and Mendeleev basin. Interesting, Schrodinger is also a high priority target for addressing several other NRC (2007) science priorities (Kring, 2009; O'Sullivan et al., 2011; Souchon et al., 2011). To assess the sites with the largest potential scientific yield, we

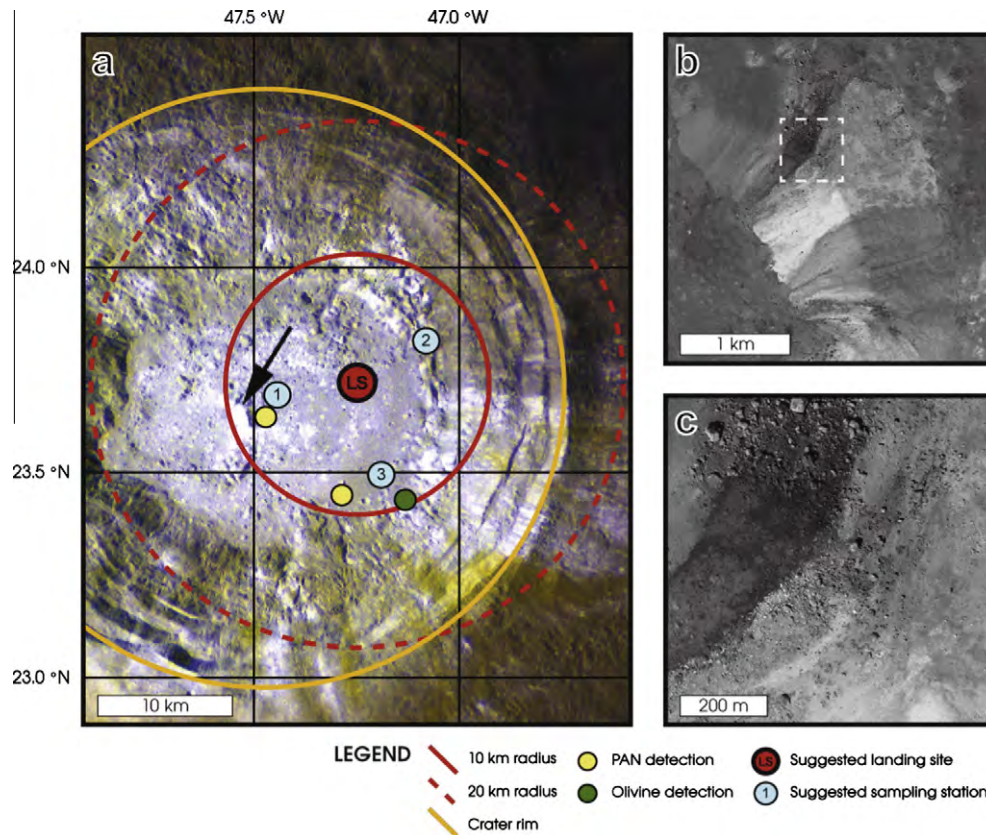


Fig. 8. (a) LROC-WAC color composite of Aristarchus crater (NASA/GSFC/Arizona State University) overlain by a suggested landing site, suggested sampling stations, as well as some recent mineral detections. The red circles show regions with 10 km radius (solid line) and 20 km radius (dashed line) with are reasonable roaming distances for a lunar rover or vehicle. The black arrow points to the center of image (b). (b) Picture depicting layering from the central peak of Aristarchus crater. The white dashed square outlines picture (c). Picture is feature from LROC image M122423410L. (c) Close up view of the layering features and albedo contrasts from image (b). (For interpretation of the references to colour in this figure legend, the reader is referred to the web version of this article.)

established a ranking system where we attribute points to each site based on the goals (3A, 3B, or both) fulfilled by that site. Sites were then ranked on the basis of their total score. Fig. 7 shows the locations of the resulting 29 preferred landing sites, which all fulfill parts of Goal 3a and non-overlapping parts of Goal 3b. Fig. 7 also points out the location of sites chosen for future GLXP lunar missions for comparison, enabling the identification of top science targets in the vicinity of proposed landing sites. Detailed studies of each of these areas can be made using our GIS. To illustrate this detailed landing site characterization process, in the next section we present case studies for two sites that rank among the top 29 of our list, and that are also relatively easy to access due to their near-side location: Aristarchus and Theophilus craters.

## 5. Two case studies

### 5.1. Aristarchus crater (23.7°N, 47.4°W, 40 km, Copernican, PKT)

The Aristarchus crater and nearby plateau show an incredibly complex mixture of geomorphologic features and lithologies. The Aristarchus region has been studied

in much detail in the literature (*e.g.*, McEwen et al., 1994; Le Mouélic et al., 2000; Chevrel et al., 1999). Being a young Copernican crater, morphologic features of Aristarchus including its walls, central peak and ejecta blanket have undergone very little erosion. The crater thus provides a fresh glimpse into the surrounding PKT region. The preserved details are apparent in recent imagery from the Lunar Reconnaissance Orbiter Camera (LROC), displaying vivid layered stratigraphy within the central peak (Fig. 8b and c).

Located within the nearside mare region, the crater would allow for sampling of a diversity of crustal rocks, including key highland and mare types. Specifically, Aristarchus penetrates into H5 highland type terrain, and is surrounded by a variety of mare types, including M2, M3 and young mare. These layers could potentially all be accessed in the central peak, provided there is no substantial erosion or weathering. Fig. 8 shows a true color image of the central peak of Aristarchus crater from the LROC instrument. This image shows distinct layering of multiple rock types. Recent analyses of spectral data hint at the presence of pure anorthosite (Ohtake et al., 2009) and of Mg-spinel bearing rocks (Dhingra et al., 2011) in the central peak. Other detections include olivine-rich exposures

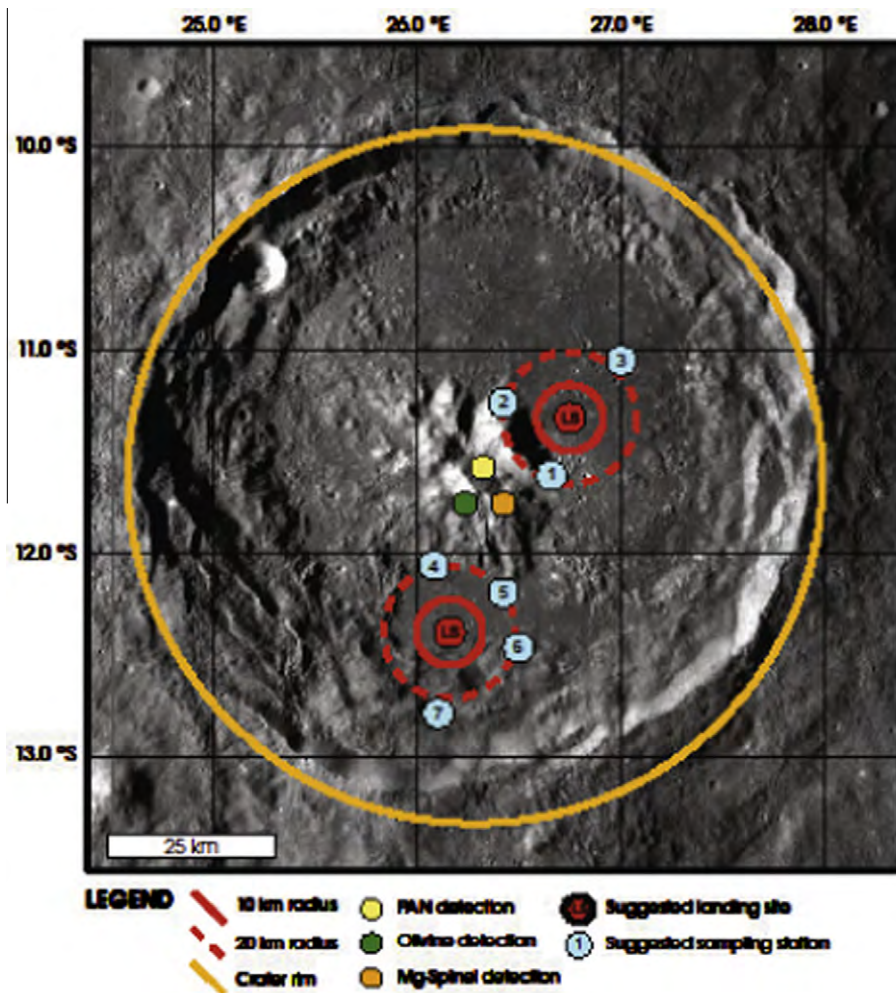


Fig. 9. LROC-WAC Mosaic centered on Theophilus crater (NASA/GSFC/Arizona State University) showing two suggested landing sites and several potential sampling locations covering the central uplift, the crater floor and the crater walls. PAN, olivine and Mg-Spinel have been detected in various amounts in the central uplift.

in a concentric region around Aristarchus crater (Yamamoto et al., 2010) as well as an olivine-enriched southern half of the crater and a low-Ca pyroxene-rich northern half (Mustard et al., 2011).

Geochemical remote sensing analysis suggests that Aristarchus crater penetrates into a KREEP-rich region of the PKT. Although Aristarchus itself is not deep enough to have primordial urKREEP material in its melt or ejecta, the young crater lies on the outskirts of the Imbrium basin, which could contain urKREEP within its ejecta blanket. Samples from Aristarchus crater will likely yield highly KREEP-enriched material, with the possibility of remnant urKREEP material from the Imbrium impact event. Any residual urKREEP exposure would occur in the uplift of the central peak or in the crater walls, as the crater would need to penetrate the topmost regolith and mare basalt. However, KREEP-basalt samples are likely to be found throughout the crater.

The region surrounding Aristarchus crater is lithologically diverse. Aristarchus crater lies on the Aristarchus

plateau, which is an uplifted block of crustal material, formed likely due to volcanic processes. The scarp of the plateau, that rises more than 2 km above Oceanus Procellarum on the southeastern margin, might be an interesting target for observing outcrops of intrusive material and layering of different lithologies. There is also evidence for pyroclastic deposits which may be sampled on the plateau, as well as a system of sinuous rilles (Rillae Aristarchus) dominated by Vallis Schröteri. Such features all suggest that that this region was dominated by volcanic processes in the past, creating a very geologically diverse terrain. Observations of possible layered structures within the central peak and exposed crater walls may provide insight into the complex volcanic and impact lithologies.

Most of the features of interest within the Aristarchus region can be observed within the central peak and exposed walls of the crater. For this reason, we suggest a landing site on the crater floor, midway between the crater walls and the central peak. However, it should be noted that the entire region outside of the crater is also of interest,

and if landing within the crater is not feasible, a site in the plateau region, especially near the scarp of the plateau, could be equally scientifically rewarding (Fig. 8).

### 5.2. *Theophilus crater (11.4°S, 26.4°E, 110km, Eratosthenian, FHTo)*

Landing and sampling at Theophilus crater would satisfy requirements to meet parts of goals 3A and 3B of the NRC report. Theophilus' central peak is mostly anorthositic (possible PAN detections), with large-scale exposures of Mg-spinel, one of only two such exposures observed to date (Dhingra et al., 2011). Smaller exposures of olivine and pyroxene-bearing materials have also been detected in the central peak (Yamamoto et al., 2010).

The location of Theophilus crater at the edge of the much larger Nectaris basin offers an interesting opportunity to sample material from much deeper in the lunar interior. As such, material that has been uplifted during the Nectaris impact event (with maximum depth of exposure of ~30 km (Whitford-Stark, 1981), could be exposed in Theophilus central peak. This may be of particular interest as Nectaris is considered one of the oldest basin-forming impact events; samples of bed rock and impact rock could help to constrain timescales of geologic processes.

An interesting landing site would be on the smooth section of the crater floor (north-east quadrant) near the central peak (Fig. 9). Samples from the central uplift would help to provide ground-truth for validating recently acquired orbital data (Kaguya, M<sup>3</sup>, LRO) and the potential depth of origin of those samples would give us invaluable insight into the composition of the lower crust, and potentially even the upper mantle.

## 6. Conclusions

This study demonstrates the use of integrated remote sensing observations as a basis to identify and characterize science-rich landing sites for lunar lander missions. Using a GIS containing many different data sets, we conclude that multiple landing sites will be required to address the entirety of goals 3A and 3B of the NRC report. We identified 29 top locations as having the potential to address several requirements within a goal, and propose specific landing sites and sampling areas for two of these locations (Aristarchus and Theophilus craters).

## Acknowledgments

The GIS was constructed by J.F., J.-F.B.-G., C.J., P.S., and A.S. during the 2010 Lunar Exploration Summer Intern Program which is supported by the NLSI Center for Lunar Science and Exploration at LPI and JSC. We are tremendously grateful to all the LPI staff for their warm welcome and precious help. We thank the organizers of the Lorenz Center Workshop 'Landing Sites for Exploration Missions' (Leiden/Noordwijk, 2011) which led to this

paper. We also thank Phil Stooke for kindly providing the information relative the GLXP preliminary landing sites. W.v.W. acknowledges financial support from a European Science Foundation EURYI award.

## Appendix A. Supplementary data

Supplementary data associated with this article can be found, in the online version, at <http://dx.doi.org/10.1016/j.asr.2012.05.020>.

## References

- Antonenko, I., Yingst, R.A. Mare and cryptomare deposits in the Schickard region of the Moon: New measurements using Clementine FeO data, in: Lunar and Planetary Science Conference XXXIII, Abstract 1438, 2002.
- Antonenko, I., Global estimates of cryptomare deposits: implications for lunar volcanism, in: Lunar and Planetary Science Conference XXX, Abstract 1703, 1999.
- Antonenko, I., Head, J.W., Mustard, J.F., Hawke, B.R. Criteria for the detection of lunar cryptomaria. *Earth Moon Planets* 69 (2), 141–172, 1995.
- Bell, J.F., Hawke, B.R. Lunar dark-haloed impact craters: origin and implications for early mare volcanism. *J. Geophys. Res.* 89 (B8), 6899–6910, 1984.
- Blanchette-Guertin, J.-F., Jilly, C.E., Flahaut, J., et al. Mission strategies for determining the vertical extent and structure of the lunar megaregolith, in: Lunar and Planetary Science Conference XLII, Abstract 1405, 2011.
- Borg, L.E., Connelly, J.N., Boyet, M., Carlson, R.W. Chronological evidence that the Moon is either young or did not have a global magma ocean. *Nature* 477, 70–72, 2011.
- Cahill, J.T.S., Lucey, P.G., Wiczorek, M.A. Compositional variations of the lunar crust: Results from radiative transfer modeling of central peak spectra. *J. Geophys. Res.* 114 (E9001), 1–17, 2009.
- Campbell, B.A., Hawke, B.R. Radar mapping of lunar cryptomaria east of Orientale basin. *J. Geophys. Res.* 110 (E9002), 1–12, 2005.
- Chevrel, S.D., Pinet, P.C., Daydou, Y., Maurice, S., Lawrence, D.J., Feldman, W.C., Lucey, P.G. Integration of the Clementine UV-VIS spectral reflectance data and the Lunar Prospector gamma-ray spectrometer data: A global-scale multielement analysis of the lunar surface using iron, titanium, and thorium abundances. *J. Geophys. Res.* 107 (E12), 1–14, 2002.
- Chevrel, S.D., Pinet, P.C., Head, J.W. The Aristarchus Plateau on the Moon: Mineralogical and structural study from integrated Clementine UV-Vis-NIR spectral data. *Icarus* 199, 9–24, 1999.
- Cintala, M.J., Grieve, R.A.F. Scaling impact melting and crater dimensions: Implications for the lunar cratering record. *Meteorit. Planet. Sci.* 33 (4), 889–912, 1998.
- Croft, S.K. The scaling of complex craters, *Proc. Lunar Planet. Sci. Conf.* 15th. *J. Geophys. Res.* 90, C828–C842, 1985.
- Croft, S.K. Cratering flow fields: implications for excavation cavities, transient cavities, and depth of excavation, in: Lunar and Planetary Science Conference XI, Abstract 1065, 1980.
- Dhingra, D., Pieters, C.M., Boardman, J.W., et al. Compositional diversity at Theophilus crater: Understanding the geological context of Mg-spinel bearing central peaks. *Geophys. Res. Lett.* 38 (L11201), <http://dx.doi.org/10.1029/2011GL047314>, 2011.
- Elkins-Tanton, L.T., Burgess, S., Yin, Q.Z. The lunar magma ocean: Reconciling the solidification process with lunar petrology and geochronology. *Earth and Planet. Sci. Lett.* 304, 326–336, <http://dx.doi.org/10.1016/j.epsl.2011.02.004>, 2011.
- Elphic, R.C., Lawrence, D.J., Feldman, W.C., Barraclough, B.L., Maurice, S., Binder, A.B., Lucey, P.G. Lunar rare earth element

- distribution and ramifications for FeO and TiO<sub>2</sub>: Lunar Prospector neutron spectrometer observations. *J. Geophys. Res.* 105 (E8), 20333–20345, 2000.
- Flahaut, J., Souchon, A.L., Blanchette-Guertin, J.-F., et al. Identification of science-rich mission sites designed to test the Lunar Magma Ocean hypothesis, in: *Lunar and Planetary Science Conference XLII*. Abstract 1844, 2011.
- Gaddis, L.R., Staid, M.I., Tyburczy, J.A., Hawke, B., Petro, N.E. Compositional analyses of lunar pyroclastic deposits. *Icarus* 161 (2), 262–280, 2003.
- Gaddis, L.R., Hawke, B., Robinson, M., Coombs, C. Compositional analyses of small lunar pyroclastic deposits using Clementine multispectral data. *J. Geophys. Res.* 105 (E2), 4245–4262, 2000.
- Garrick-Bethell, I., Nimmo, F., Wicczorek, M. Structure and formation of the lunar farside highlands. *Science* 330, 949–951, 2010.
- Giguere, T.A., Hawke, B.R., Blewett, D.T. Cryptomare and pyroclastic deposits in the Gassendi region of the Moon, in: *Lunar and Planetary Science Conference XXXVIII*. Abstract 1132, 2007.
- Giguere, T.A., Hawke, B.R., Blewett, D.T., Bussey, D.B.J., Lucey, P.G., Smith, G.A., Spudis, P.D., Taylor, G.J. Remote sensing studies of the Lomonosov-Fleming region of the Moon. *J. Geophys. Res.* 108 (E11), 1–14, 2003.
- Gillis, J.J., Jolliff, B.L., Korotev, R.L. Lunar surface geochemistry: Global concentrations of Th, K, and FeO as derived from Lunar Prospector and Clementine data. *Geochim. Cosmochim. Acta* 68 (18), 3791–3805, 2004.
- Greeley, R., Kadel, S.D., Williams, D.A., et al. Galileo imaging observations of lunar maria and related deposits. *J. Geophys. Res.* 98 (E9), 17183–17205, 1993.
- Haruyama, J., Ohtake, M., Matsunaga, T., et al. Long-lived volcanism on the lunar farside revealed by Selene terrain camera. *Science* 323 (5916), 905–908, 2009.
- Haskin, L.A., Gillis, J.J., Korotev, R.L., Jolliff, B.L. The materials of the lunar Procellarum KREEP terrane: A synthesis of data from geomorphological mapping, remote sensing, and sample analyses. *J. Geophys. Res.* 105 (E8), 20403–20415, 2000.
- Hawke, B.R., Gillis, J.J., Giguere, T.A., et al. The earliest mare basalts, in: *Lunar and Planetary Science Conference XXXVI*. Abstract 1642, 2005a.
- Hawke, B.R., Gillis, J.J., Giguere, T.A., et al. Remote sensing and geologic studies of the Balmer-Kapteyn region of the Moon. *J. Geophys. Res.* 110 (E06004), 1–16, 2005b.
- Hawke, B.R., Peterson, C.A., Blewett, D.T., et al. Distribution and modes of occurrence of lunar anorthosite. *J. Geophys. Res.* 108 (E6), 1–16, 2003a.
- Hawke, B.R., Blewett, D.T., Bussey, D.B.J., et al. Geochemical anomalies in the lunar highlands, in: *Lunar and Planetary Science Conference XXXIV*. Abstract 1198, 2003b.
- Heather, D.J., Dunkin, S.K. A stratigraphic study of southern Oceanus Procellarum using Clementine multispectral data. *Planet. Space Sci.* 50 (14–15), 1299–1309, 2002.
- Hiesinger, H., Head, J., Wolf, U. Ages of mare basalts on the lunar nearside: a synthesis, in: *Lunar and Planetary Science Conference XXXIX*, Abstract 1269, 2008.
- Hiesinger, H., Head III, J., Wolf, U., et al. New ages for basalts in Mare Fecunditatis based on crater size-frequency measurements, in: *Lunar and Planetary Science Conference XXXVII*. Abstract 1151, 2006.
- Hiesinger, H., Head, J.W., Wolf, U., et al. Ages and stratigraphy of mare basalts in Oceanus Procellarum, Mare Nubium, Mare Cognitum, and Mare Insularum. *J. Geophys. Res.* 108 (1), 1–27, 2003.
- Hiesinger, H., Jaumann, R., Neukum, G., et al. Ages of mare basalts on the lunar nearside. *J. Geophys. Res.* 105 (E12), 29239–29275, 2000.
- Jilly, C.E., Sharma, P., Souchon, A.L., et al. Lunar landing sites to explore the extent of KREEP and its significance to key planetary processes, in: *Lunar and Planetary Science Conference XLII*. Abstract 1270, 2011.
- Jolliff, B.L., Wiseman, S.A., Lawrence, S.J., et al. Non-mare silicic volcanism on the lunar farside at Compton–Belkovich. *Nature Geosci.* <http://dx.doi.org/10.1038/ngeo1212>, 2011.
- Jolliff, B.L., Wicczorek, M.A., Shearer, C.K., et al. *New Views of the Moon. Reviews in Mineralogy and Geochemistry*, vol. 60. Mineralogical Society of America, Washington, DC, 772 p., 2006.
- Jolliff, B.L., Gillis, J.J., Haskin, L.A., et al. Major lunar crustal terranes: surface expressions and crust-mantle origins. *J. Geophys. Res.* 105 (E2), 4197–4216, 2000.
- Jutzi, M., Asphaug, E. Forming the lunar farside highlands by accretion of a companion moon. *Nature* 476 (7358), 69–72, 2011.
- Kring, D.A. Targeting complex craters and multi-ring basins to determine the tempo of impact bombardment while simultaneously probing the lunar interior, in: *Lunar Reconnaissance Orbiter Science Targeting Meeting*. Abstract 6037, 2009.
- Lawrence, D.J., Feldman, W.C., Elphic, R.C., et al. Iron abundances on the lunar surface as measured by the Lunar Prospector gamma-ray and neutron spectrometers. *J. Geophys. Res.* 107 (E12), 5130, <http://dx.doi.org/10.1029/2001JE001530>, 2002.
- Lawrence, D.J., Feldman, W.C., Barraclough, B.L., et al. Global elemental maps of the Moon: The Lunar Prospector gamma-ray spectrometer. *Science* 281 (5382), 1484–1489, 1998.
- LEIP, Lunar Exploration Intern Program. *The Moon as an Accessible Laboratory for Studying the Impact Process on Planetary Scales: Assessing Concept 6 of the NRC Report on the Scientific Context for the Exploration of the Moon*, Lunar and Planetary Institute, Houston, Texas, in electronic format at the Lunar and Planetary Institute, Houston, 2010.
- Le Mouélic, S., Langevin, Y., Erard, et al. Discrimination between maturity and composition of lunar soils from integrated Clementine uv-visible/near infrared data: application to the Aristarchus plateau. *J. Geophys. Res.* 105 (E4), 9445–9455, 2000.
- Losiak, A., Wilhelms, D.E., Byrne, C.J., et al. A new lunar impact crater database, in: *Lunar and Planetary Science Conference XL*. Abstract 1532, 2009.
- Lucey, P., Korotev, R.L., Gillis, J.J., et al. Understanding the lunar surface and space-Moon interactions, in: Jolliff, B.L., Wicczorek, M.A., Shearer, C.K., Neal, C.R. (Eds.), *New Views of the Moon, Reviews in Mineralogy and Geochemistry*, vol. 60. Mineral. Soc. America, Washington, DC, pp. 83–219, 2006.
- Lucey, P.G., Blewett, D.T., Jolliff, B.L. Lunar iron and titanium abundance algorithms based on final processing of Clementine ultraviolet-visible images. *J. Geophys. Res.* 105 (E8), 20297–20305, 2000.
- Lucey, P.G., Blewett, D.T., Hawke, B.R. Mapping the FeO and TiO<sub>2</sub> content of the lunar surface with multispectral imagery. *J. Geophys. Res.* 103 (E2), 3679–3699, 1998.
- Maxwell, D.E. Simple Z model of cratering, ejection, and the overtuned flap. In: Roddy, D.J., Pepin, R.O., Merrill, R.B. (Eds.), *Impact and Explosion Cratering*. Pergamon, Elmsford, New York, pp. 1003–1008, 1977.
- McEwen, A.S., Robinson, M.S., Eliason, E.M., et al. Clementine observations of the Aristarchus region of the Moon. *Science* 266 (5192), 1858–1862, 1994.
- Melosh, H.J. *Impact Cratering: A Geologic Process*. Oxford University Press, 245 p., 1989.
- Mustard, J.F., Pieters, C.M., Isaacson, P.J., et al. Compositional diversity and geologic insights of the Aristarchus crater from Moon Mineralogy Mapper data. *J. Geophys. Res.* 116, E00G12, [doi:10.1029/2010JE003726](http://dx.doi.org/10.1029/2010JE003726), 2011.
- Neukum, G., Ivanov, B.A. Crater size distributions and impact probabilities on Earth from lunar, terrestrial-planet, and asteroid cratering data, in: Gehrels, T., Matthews, M.S., Schumann, A.M. (Eds.), *Hazards Due to Comets and Asteroids*, The University of Arizona Press. pp. 359–416, 1994.
- NRC, National Research Council. *Scientific Context for the Exploration of the Moon: A National Research Council space science board study*. Space Resources Roundtable VIII, 107 p., 2007.
- Nyquist, L.E., Bogard, D.D., Shih, C.Y. Radiometric chronology of the Moon and Mars, in: Bleeker, J.A.M., Geiss, J., Huber, M.C.E. (Eds.), *The Century of Space Science*. Kluwer Academic Publishers. pp. 1325–1376, 2001.

- Nyquist, L.E., Shih, C.Y., Reese, Y.D., et al. Lunar crustal history recorded in lunar anorthosites, in: Lunar and Planetary Science Conference XL. Abstract 1383, 2010.
- Ohtake, M., Matsunaga, T., Haruyama, J., et al. The global distribution of pure anorthosite on the Moon. *Nature* 461 (7261), 36–241, 2009.
- Ohtake, M., Mastunaga, T., Takeda, H., et al. Distribution of purest anorthosite on the entire lunar surface, in: Lunar and Planetary Science Conference XL. Abstract 1628, 2010.
- O'Sullivan, K.M., Kohout, T., Thaisen, K.G., et al. Calibrating several key lunar stratigraphic units representing 4 billion years of lunar history within Schrödinger basin, in: Williams, D.A., Ambrose, W. (Eds.), *Recent Advances in Lunar Stratigraphy*. Geological Society of America Special Paper, Boulder, CO., pp. 117–128, 2011.
- Parmentier, E.M., Zhong, S., Zuber, M.T. Gravitational differentiation due to initial chemical stratification: origin of lunar asymmetry by the creep of dense KREEP. *Earth Planet. Sci. Lett.* 201 (3–4), 473–480, 2002.
- Pieters, C., Boardman, J., Buratti, B. Identification of a new spinel-rich lunar rock type by the Moon Mineralogy Mapper (M3), in: Lunar and Planetary Science Conference XLI. Abstract 1854, 2010.
- Pieters, C., Head III, J.W. Extent of basaltic volcanism in South Pole-Aitken basin, in: Lunar and Planetary Science Conference XXXII. Abstract 1821, 2001a.
- Pieters, C.M., Gaddis, L., Jolliff, B., et al. Rock types of South Pole-Aitken basin and extent of basaltic volcanism. *J. Geophys. Res.*, 106(E11), pp. 8001–28022, 2001b.
- Pieters, C.M., Staid, M.I., Fischer, E., et al. A sharper view of impact craters from Clementine data. *Science* 266 (5192), 1844–1848, 1994.
- Pieters, C. Bullialdus – strengthening the case for lunar plutons. *Geophys. Res. Lett.* 18 (11), 2129–2132, 1991.
- Pieters, C. Composition of the Lunar Highland Crust From Near-Infrared Spectroscopy. *Rev. Geophys.* 24 (3), 557–578, 1986.
- Robinson, M.S., Brylow, S.M., Tschimmel, M. Lunar Reconnaissance Orbiter Camera (LROC) instrument overview. *Space Sci. Rev.* 150, 81–124, <http://dx.doi.org/10.1007/s11214-010-9634-2>, 2010.
- Ryder, G. Lunar sample 15405: Remnant of a KREEP basalt-granite differentiated pluton. *Earth Planet. Sci. Lett.* 29 (2), 255–268, 1976.
- Schultz, P.H., Spudis, P.D. Evidence for ancient mare volcanism, in: Lunar and Planetary Science Conference Proceedings, vol. 10, pp. 2899–2918, 1979.
- Sharma, P., Blanchette-Guertin, J.F., Jilly, C.E., et al. Identifying lunar landing sites for sampling lower crust and mantle material, in: Lunar and Planetary Science Conference XLII. Abstract 1579, 2011.
- Shearer, C.K., Hess, P.C., Wiczorek, M.A., et al. Thermal and magmatic evolution of the Moon. In: Jolliff, B.L., Wiczorek, M.A., Shearer, C.K., Neal, C.R. (Eds.), *New Views of the Moon*. Reviews in Mineralogy and Geochemistry, vol. 60. Mineral. Soc. America, Washington, DC. pp. 365–518, 2006.
- Shervais, J.W., Taylor, L.A. Petrologic constraints on the origin of the Moon, in: Hartmann, W.K., et al. (Eds.) *Origin of the Moon*. Lunar Planet. Inst., Houston, TX. pp. 173–201, 1986.
- Smith, D.E., Zuber, M.T., Neumann, G.A., et al. Initial observations from the Lunar Orbiter Laser Altimeter (LOLA). *Geophys. Res. Lett.* 37, L18204, <http://dx.doi.org/10.1029/2010GL043751>, 2010.
- Snyder, G.A., Taylor, L.A., Halliday, A.N. Chronology and petrogenesis of the lunar highlands alkali suite: Cumulates from KREEP basalt crystallization. *Geochim. Cosmochim. Acta* 59 (6), 1185–1203, 1995.
- Snyder, G.A., Taylor, L.A., Neal, C.R. A chemical model for generating the sources of mare basalts: combined equilibrium and fractional crystallization of the lunar magmasphere. *Geochem. Cosmochim. Acta* 56, 3809–3823, 1992.
- Souchon, A.L., Flahaut, J., Sharma, P., et al. Suggested landing sites to study key planetary processes on the Moon: the case of Schrödinger basin, in: Lunar and Planetary Science Conference XLII. Abstract 1791, 2011.
- Spudis, P.D., Davis, P.A. A chemical and petrological model of the lunar crust and implications for lunar crustal origin, in: Lunar and Planetary Science Conference Proceedings, vol. 17, pp. 84–90, 1986.
- Stöffler, D. Cratering mechanics: data from terrestrial and experimental craters and implications for the Apollo cratering mechanics: data from terrestrial and experimental craters and implications for the Apollo 16 site, in: James, O.B. (Ed.), *Workshop on Apollo 16*, pp. 132–141, 1981.
- Sunshine, J., Besse, S., Petro, N. Hidden in plain sight: spinel-rich deposits on the nearside of the Moon as revealed by Moon Mineralogy Mapper (M3), in: Lunar and Planetary Science Conference XLI. Abstract. 1508, 2010.
- Taylor, S.R. *Planetary Science: A Lunar Perspective*. Lunar and Planetary Institute, Houston, TX, 81 p., 1982.
- Terada, K., Anand, M., Sokol, A.K., et al. Cryptomare magmatism 4,35 Gyr ago recorded in lunar meteorite Kalahari 009. *Nature* 450 (7171), 849–852, 2007.
- Tompkins, S., Pieters, C.M. Mineralogy of the lunar crust: results from Clementine. *Meteorit. Planet. Sci.* 34 (1), 25–41, 1999.
- Tompkins, S. Mafic plutons in the lunar highland crust, in: Lunar and Planetary Science Conference XXIX. Abstract 1656, 1998.
- Tyrie, A. Age dating of mare in the lunar crater Tsiolkovsky by crater-counting method. *Earth Moon Planet.* 42 (3), 245–264, 1988.
- Warren, P.H. “New” lunar meteorites: Implications for composition of the global lunar surface, lunar crust, and the bulk Moon. *Meteorit. Planet. Sci.* 40 (3), 477–506, 2005.
- Warren, P.H., Kallemeyn, G.W. The MacAlpine Hills lunar meteorite and implications of the lunar meteorites collectively for the composition and origin of the Moon. *Geochim. Cosmochim. Acta* 55, 3123–3138, 1991.
- Warren, P.H., Kallemeyn, G.W. Lunar meteorites: constraints on lunar composition and evolution, in: Lunar and Planetary Science Conference XIX. Abstract 1236, 1988.
- Warren, P.H. The magma ocean concept and lunar evolution. *Annu. Rev. Earth Planet. Sci.* 13 (1), 201–240, 1985.
- Warren, P.H., Wasson, J.T. The origin of KREEP. *Rev. Geophys. Space Phys.* 17 (1), 73–88, 1979.
- Warren, P.H., Wasson, J.T. Pristine nonmare rocks and the nature of the lunar crust, in: *Proc. Lunar Sci. Conf.*, 8th, 2215–2235, 1977.
- Werner, S.C., Medvedev, S. The Lunar rayed-crater population – characteristics of the spatial distribution and ray retention. *Earth Planet. Sci. Lett.* 295 (1–2), 147–158, <http://dx.doi.org/10.1016/j.epsl.2010.03.036>, 2010.
- Wichman, R.W., Schultz, P.H. Crater-centered laccoliths on the Moon: Modeling intrusion depth and magmatic pressure at the crater Tarantius. *Icarus* 122 (1), 193–199, 1996.
- Wiczorek, M.A., Jolliff, B.L., Khan, A., et al. The constitution and structure of the lunar interior. in: Jolliff, B.L., Wiczorek, M.A., Shearer, C.K., Neal, C.R. (Eds.), *New Views of the Moon*. Reviews in Mineralogy and Geochemistry, vol. 60. Mineral. Soc. America, Washington, DC, pp. 221–364, 2006.
- Wiczorek, M.A., Zuber, M.T. The composition and origin of the lunar crust: Constraints from central peaks and crustal thickness modeling. *Geophys. Res. Lett.* 28 (21), 4023–4026, 2001.
- Wiczorek, M.A., Phillips, R.J. The “Procellarum KREEP terrane” – implications for mare volcanism and lunar evolution. *J. Geophys. Res.* 105(E8), 20417–20430, 2000.
- Wiczorek, M.A., Phillips, R.J. Potential anomalies on a sphere: applications to the thickness of the lunar crust. *J. Geophys. Res.* 103(E1), 1715–1724, 1998.
- Wilhelms, D.E. *Geologic History of the Moon*. US Geol. Surv. Prof. Pap., 1348, 302 pp., 1987.
- Whitford-Stark, J.L. The evolution of the lunar Nectaris multiring basin. *Icarus* 48(3), 393–427, [http://dx.doi.org/10.1016/0019-1035\(81\)90053-1](http://dx.doi.org/10.1016/0019-1035(81)90053-1), 1981.

- Wöhler, C., Lena, R. Lunar intrusive domes: Morphometric analysis and laccolith modeling. *Icarus* 204 (2), 381–398, 2009.
- Wood, J.A. Bombardment as a cause of the lunar asymmetry. *Earth Moon Planet.* 8, 73–103, 1973.
- Wood, J.A., Dickey, J.S., Marvin, U.B., et al. Lunar anorthosites and a geophysical model of the Moon, in: *Proceedings of the Apollo 11 Lunar Science Conference*, vol. 1. pp. 965–988, 1970.
- Yamaguchi, A., Karouji, Y., Takeda, H., et al. The variety of lithologies in the Yamato-86032 lunar meteorite: Implications for formation processes of the lunar crust. *Geochim. Cosmochim. Acta* 74, 4507–4530, 2010.
- Yamamoto, S., Nakamura, R., Matsunaga, T., et al. Possible mantle origin of olivine around lunar impact basins detected by Selene. *Nat. Geosci.* 3 (7), 1–4, 2010.